FACULDADE DE ENGENHARIA DA UNIVERSIDADE DO PORTO

U.PORTO

FEUP **FACULDADE DE ENGENHARIA**
UNIVERSIDADE DO PORTO

Automated Detection of Bone structure Keypoints on Magnetic Resonance Imaging - Sternum and Clavicles

Beatriz Gonçalves Rocha

MESTRADO INTEGRADO EM BIOENGENHARIA - ENGENHARIA BIOMÉDICA

Supervisor: Hélder Filipe Pinto de Oliveira

Co-Supervisor: João Pedro Fonseca Teixeira

October 29, 2018

Abstract

Breast cancer is one of the most prevalent types of carcinogenic diseases worldwide, meaning that is a pathology very appealing to be explored in terms of cure and methods to help the diagnose and treatment processes.

With the evolution of technology applied to science, much work has been developed in order to find solutions to improve the treatments of pathologies like breast cancer. One of those, relates to this dissertation work, where a strategy for personalized surgical treatment is being explored in order to increase the quality of life for the patients who have to be submitted to oncoplastic surgical procedures.

This dissertation work, focuses on the automatic segmentation of the Sternum and the Clavicles in Magnetic Resonance Imaging (MRI). The identification of these specific bones will be used as reference to help a three dimensional reconstruction of patient digital model through their individual MRI acquisition. To achieve this, is important to have body structures identified in the acquisitions such as bones to serve as reference to create the individual radiological atlas and multi-modal fusion.

The segmentation of this structures proposed is achieved using the gradient of the images elliptically transformed, where the boundaries are emphasized. The minimum cost pixel path, after an intensity modification, is estimated and corresponds to the object contours. Classification approaches using Support Vector Machine and Random Forest models were also tested, using different sets of features extracted.

The dataset used in this work had 14 MRI T1-weighted breast cancer patient acquisitions, from their thoracic area. The classification methods for the sternum the clavicles achieved Dice Similarity Coefficient (DSC) of 0.087 and 0.25. In the gradient based segmentation the DSC was 0.58 for the sternum and 0.36 for clavicles.

The developed method, based on image gradient to detect the objects after being transformed, revealed to be a great disclosure to achieve the sternum and clavicles automated detection in MRI. It is a promising starting point to develop a robust segmentation method for these bones.

ii

Acknowledgements

This dissertation represents the culmination of long five years.

They were certainly the most intense years of my life, so far, and I am grateful that I embrace this opportunity.

I would like to thank all my Professors. Beginning in my Pre and Elementary school teachers, Leninha and Susana, to every High School and University Professors. All of you, somehow, taught me something that I will carry for my life.

I would also like to thank all my friends, especially the ones that had to deal with me and my moods during this process. Thank you for cheering me up, even in my darkest days. I know it was not easy, but I at least hope it was funny.

I would also like to give a special thanks to my friends who welcome me in my first days in university. Those were not easy days, with many doubts and insecurities about my choices, but with your help I managed to finish my degree in five years!

At last, but definitely not least important, I would like to give the biggest thanks my family. Without them I would never have the possibility to even dream to achieve this. My real, Marcos and Mizé, and fake uncles, Amélia e João for always be there for me, when I needed the most. My cousin, Mariana, for being my partner in everything during this past year. Also, my grandparents, Alice and Rodolfo who accommodate me and my bad moods and always missed me when I was not home, and my grandfather Henrique for always support me during weekend quick visits and lunches. My stepmother, Zélia for the understanding about dealing with engineering courses. My brother, Francisco, who grow up watching me studying to achieve this. Thank you for all the times you distract me and made me realize that there are things much more important and unique than work. I hope I will help you in your journey even more than you helped me. My mother and father! Without whom I could not even image to pass the elementary school. I want to give you the biggest thank you, from the bottom of my heart, for all the support. Despite every distance, you were always there for me. Thank for not giving up on me and on my insecurities, tears, mournings and fears. I hope I made and will always make you proud!

All of you shaped the person I become today. I don't know what is coming next, but I hope I will count on you for many years more and you will help me reaching other things that seem impossible for me now to accomplish.

Beatriz Gonçalves Rocha.

"Science works on the frontier between knowledge and ignorance.
We're not afraid to admit what we don't know.
There's no shame in that.
The only shame is to pretend that we have all the answers."

Neil deGrasse Tyson, Cosmos: A Spacetime Odyssey.

Contents

List of Figures

List of Tables

Abbreviations and Symbols

2D	Two Dimensional
3D	Three Dimensional
AAM	Active Appearance Model
ASM	Active Shape Model
AvgD	Average Distance
BCCT	Breast Cancer Conserving Therapy
CT	Computed Tomography
DRLSE	Distance Regularized Level Set Evolution
DSC	Dice Similarity Coefficient
FN	False Negative
FP	False Positive
GAC	Geodesic Active Contours
GC	Graph minimum-Cut
GLCM	Grey-Level Co-occurrence Matrix
k-NN	k Nearest Neighbors
LDA	Linear Discriminant Analysis
LWV	Locally Weighted Vote
MR	Magnetic Resonance
MRI	Magnetic Resonance Imaging
MSE	Mean Square Error
PDM	Point Distribution Model
RF	Random Forest
RG	Region Growing
RMSD	Root Mean Square Distance
ROI	Region of Interest
Sens	Sensitivity
SNR	Signal to Noise Ratio
Spec	Specificity
SSM	Statistic Shape Model
SVM	Support Vector Machine
TN	True Negative
TP	True Positive

Chapter 1

Introduction

1.1 Context

Breast cancer is one of the most common types of cancer worldwide. Among female population, is the most prevalent cause of death as a non-skin type of cancer. The statistics from 2012 indicated that there were about 1.60 million new diagnoses and 0.52 million deaths caused by this type of cancer. Demographic changes related to the population growth and regional risks are indicated as the main factors to the increasing of the disease burden (Figure 1.1) .
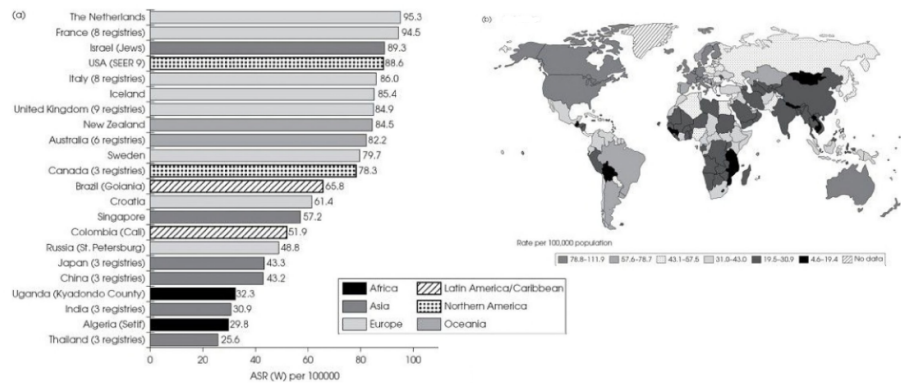
Figure 1.1: Global distribution estimated age-standardized of female breast cancer (a) and its incidence worldwide (b) Imaging [2018].

Being the incidence higher in Western countries, the burden of the disease is major located in East and Central Asia, with 41.5% of deaths and 36.3% of the cases. In Europe, the statistics for diagnosis and deaths is about 25%. In general, though the years between 1994 and 2012 the incidence of the cancer has been increasing 0.6% per year between women at ages of 20 to 39. The mortality rate has been declining due to the combination of treatment improvements and the early detection but still high: 21.52%. The risks of developing this cancer relies mainly on the genetic predisposition and some habits like the alcohol consumption and unhealthy weight [Imaging, 2018].

Cancer is characterized as being the presence of a malignant tumor, which is an abnormal development of cells that creates a mass of tissue. There are a few treatments available nowadays to try to eliminate that, being its early detection and treatment options largely studied. Many of the treatments rely on chemical attack to the tumor, however some patients still need to fight it physically, removing the tumor itself. In the case of breast surgery, it is removed part or the entire breast where the tumor relies, in order to help to overcome the pathology.

The decisions to be made concerning the treatment are numerous, complex and differ from patient to patient. They still rely almost exclusively on the perspective of the surgeon, concerning the post-surgical aesthetic result.

1.2   Motivation

The fact that the breast cancer mortality rates have been decreasing, makes that many survivors still have to deal with the consequences of the disease treatment for a considerable amount of their lives. In particular, the breast surgery consequences usually are related with the psychological recovery which can be compromised if the patient rejects or stays unsatisfied with the aesthetic result.

Breast cancer conservative treatment (BCCT) came as an alternative to the traditional mastectomy, having the main objective of locally control the tumor, having the same positive results of the traditional surgery but taking in consideration a satisfactory aesthetic result.

Some decisions concerning the surgery remain on the physician's perspective, leading sometimes to unsatisfactory outcomes due to the fact of being a quite subjective analysis due to the lack of concrete visualization of the anatomical condition of the patient and the lack of methods to keep the patient involved in the process.

An objective evaluation of the process and its results would improve these techniques, increasing the objectivity, reproducibility and the communication between the physician and the patient.

Developing a three dimensional (3D) individual model of the breast area enables the achievement of a better perspective on the surgical options and their consequences, being an evident alternative to the current methodology. It would allow a better surgery planning, giving the digital model of the body structures through a large number of angles. I would also provide a volume/volume deficit estimation and it would allow the patients to get more involved and understand better the procedures and the possible results [Oliveira et al., 2014].

The conceptualization of this 3D model relies on the digital reconstitution of the patient body structures based on their Magnetic Resonance (MR) images. Together with an external reconstitution, the inner parts of the body have to be connected with the external ones. To achieve that, it is necessary an automatic identification of some keypoints in the MRI acquisitions to connect these two reconstituted parts of the patient. With this kind of personalized model, it would provide tools to perform the digital examination and surgery planning in a more objective and realist way.

1.3 Objectives

This dissertation work was developed in line with the goals of the Portugal2020 BCCT.Plan Project, where tools for clinical teams are being built and different strategies for personalized surgical treatment for patients are being explored. This will allow to adjust and plan each surgery. This project is inserted in a three years partnership between INESC TEC, the Champalimaud Foundation and NEADVANCE.

It will take in consideration the MR images from each oncologic breast patients that were subjected to an oncoplastic surgery. From this scan, there are many structures that can be detected in those images. Some can be considered as references for the 3D reconstruction, working as key points to guide the digital model creation.

In this dissertation, the human skeleton is the main part considered. In particular, the Clavicles and the Sternum automatic detection is the main objective of this work. The detection of these bones will help in the reconstitution of each 3D model, giving reference keypoints to provide the precision of multi-modal registration tasks. As they are the most superficial bones, in this area, they will support the connection of the most external reconstituted body parts with the internal content.

1.4 Contributions

With this dissertation work, it is expected to develop a technique to automatically identify the sternum and the clavicles in T1-weighted MR volumes which will constitute a new tool to help achieve the main research line objectives of the project where this dissertation is inserted. The automatic detection of this structures will provide the model in development key points to serve as reference in the process of transformation the MRI acquisitions into a digital 3D model.

A scientific paper was also written, focusing on the sternum segmentation. This achievement also has the potential to be a new approach in the biomedical imaging science field, since the most common techniques for bone chest detection use X-Ray images. This method can become useful for other applications where the detection of this bones in MRI is necessary or even to serve as inspiration for other object detection in similar conditions.

1.5 Structure

The present document is a dissertation work. It is divided in the following chapters and topics:

The Chapter 2, has two main sections. The Background is where the main concepts that support the whole work are explained and described. In the section of the Segmentation Techniques the algorithms already described in the literature, that are somehow related to this work, are presented and the ones that can be more relevant for the desired implementation are explained. At the end of this chapter, a brief summary is made.

In Chapter 3 it is made a short introduction to contextualize the implementation process. Classification methods applied during the dissertation work are exposed. The last section is the description of the gradient based method, which explains an algorithm developed to segment each structure (sternum and clavicles) to achieve the intended objective.

In Chapter 4 an initial characterization of the dataset that was used to test the algorithms is made. Then, the results are exposed through tables with statistical measures used to evaluate the performance of the methods and some visual examples are also exposed. After that, the results are explained and justified during the Discussion section.

In the final Chapter, 5, the conclusions of the work developed are made and the possible future approaches and improvements are referred.

Chapter 2

Literature Review

2.1 Medical and Anatomical Background

It is important to understand the theoretical components of the topics that are going to be addressed during this dissertation work to understand better its characteristics, the way the structures appear in the images, their shape and constitution and the technique involved in their acquisition.

2.1.1 Bone Structure

Bone is a hard connective tissue with matrix (mineralized) and cells (living part). Its matrix consists of collagen fibers, the organic portion, and hydroxyapatite, the inorganic portion containing calcium and phosphate.

There are two types of bone structure: the compact and the cancellous one. The compact bone is composed by osteons, it is hard and dense, making the outside surface and the shaft of long bones. The spongy one has a thin and irregular shaped plate called trabeculae, arranged in a lattice work, being less dense.

Bones have rich blood supply which provides them the capacity to repair themselves quicker than other parts like cartilage [Rod Seeley and Philip Tate, 2003].

2.1.2 Skeletal System

The skeletal system is constituted by all of the bones and joints present in the whole body, being the solid framework that supports, protects and anchors the rest of the body parts. It has two distinctive portions: the axial and the appendicular skeleton, being the axial constituted by a total of eighty bones. It includes the vertebral column, the rib cage and the skull. The appendicular has a total of one hundred and twenty-six bones composed by the remaining ones.

The skeleton acts as a scaffold to provide support, it protects organs and the soft tissues that surrounds, it is an attachment points provider for muscles allowing movement at the joints and it also owns nerves and the production of new cells that occurs in the red marrow. It is located inside of bones in their medulla cavities, transforming in yellow bone marrow through adulthood

and storing energy in lipidic forms. It also stores different type of essential elements like calcium, iron and and hormones to help the growth and body repair.

The skeleton expands throughout childhood being the foundation for the other body parts to grow along with. It begins to form in fetal development as a hyaline cartilage and dense irregular connective tissue which makes the structure flexible being a soft framework and a placeholder for the future replacement osseous tissue (calcification)[Rod Seeley and Philip Tate, 2003, Ken Saladin, 2003].

2.1.3   Sternum

The sternum is a component of the thoracic cage region of the skeleton, as represented in the Figure 2.3, articulating with the right and left clavicle and some ribs. It is a long, narrow flat bone located at the anterior aspect of the thorax and the heart, lies in the mid-line of the chest and has a shape roughly similar to a "T". It is composed by three pieces: the manubrium, the body and the xiphoid process (Figure 2.2).

In average, a sternum has about 15 to 20 centimeters length, and 2.5 centimeters wide and thick, and it is a bone mainly spongious and highly vascularized due to the presence of red marrow in its interior. The sternum is commonly known as the breastbone, since it serves as keystone for the rib cage, connecting with it, and stabilizes the thoracic skeleton. It also gives protection for several vital components located in the chest such as the heart, lungs, thymus gland, aorta and vena cava. There are many muscles that allow movements of the arms, neck and head that derive from the sternum.
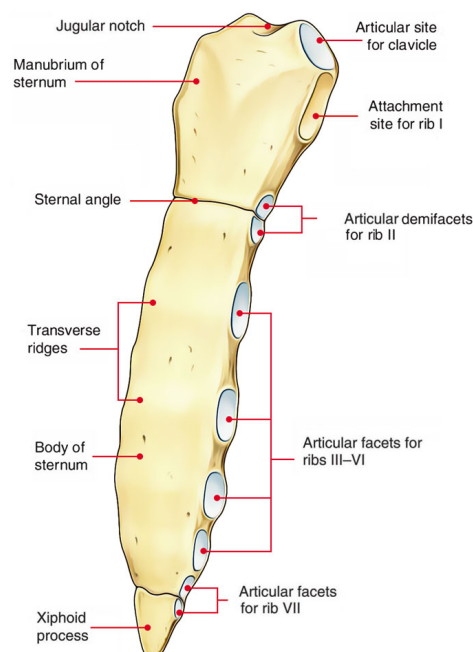
Figure 2.1: Ken Saladin [2003] representation of Sternum

The manubrium part has a superior concave shape, with a depression denominated as jugular notch which articulates with the medial ends of the clavicles to form the sternoclavicular joints. On the lateral edges of the manubrium, there is a facet that articulates with the costal cartilage of the first rib and a demifacet to articulate with part of the costal cartilage of the second rib. In the lowest part it forms the sternal angle to articulate with the body part of sternum.

The body is the longest part of the sternum and has an irregular rectangular shape. Some costal cartilages of ribs, starting from the second one, connect there forming the bulk of the rib cage. Also, in this part are slight indentations, the articular facets, to provide the attachment points for the costal cartilages, preventing rib separation.

The xiphoid process is the smallest and the most inferior region of the sternum and it has a variable shape and size. It is not always an ossified part of the body: in the early life stays as a flexible hyaline cartilage region and ossifies throughout childhood and adulthood until around the age of 40 when all its cartilage is replaced by bone. Regardless of its degree of ossification, serves as an important point for attachment diaphragm tendons and of abdominal muscles such as rectus abdominis, and transversus abdominis [Rod Seeley and Philip Tate, 2003, Ken Saladin, 2003].

2.1.4 Clavicle

The clavicle is a slender bone, as represented in the Figure 2.3, classified as a long bone having a slightly "S" shape. It has three main functions: attachment, protection and force transmission. Being convex in the medial aspect from the front view and concave from the lateral, it is crucial to sustain the forces applied from the pectoralis muscles and can be divided in two ends (the sternal and the acromial) and a shaft.
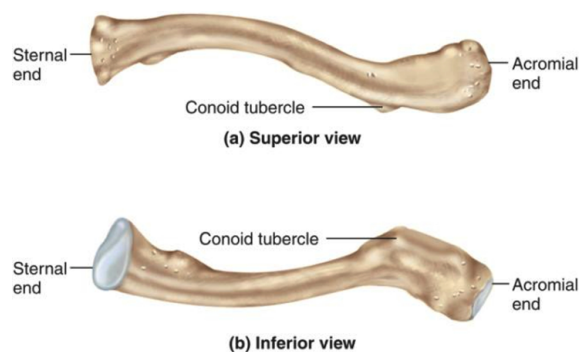
Figure 2.2: Ken Saladin [2003] representation of Clavicles

The sternal end contains a facet to articulate with the manubrium of the sternum in the sternoclavicular joint. It has a rough oval depression in the inferior surface for the costoclavicular ligament. The acromial end has a small facet to articulate with acromion of the scapula and serves as attachment for two ligaments: the conoid tubercle and the trapezoid line.

It is doubly present in a normal human body, being each clavicle (right and left) connected to the sternum by their sternal ends [Ken Saladin, 2003, Rod Seeley and Philip Tate, 2003].
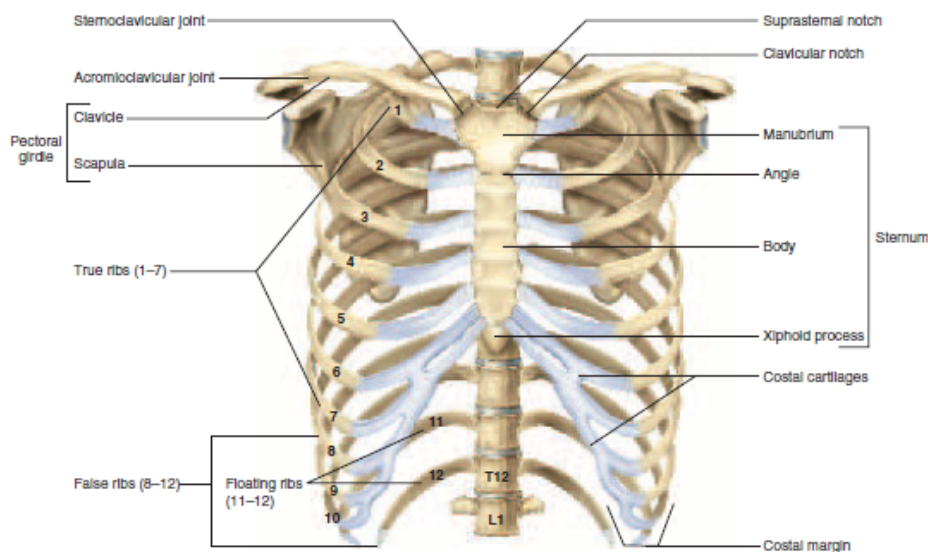
Figure 2.3: Ken Saladin [2003] representation of the Thoracic Cage and Pectoral Girdle

2.1.5   Magnetic Resonance Imaging

Magnetic Resonance (MR) was firstly developed as a superior computed tomography (CT) scanning technique, in 1970s, to visualize soft tissues.

By definition, magnetic resonance is a property of the elements that when submitted to a magnetic strong field and excited by radio waves in a specific frequency (Lamor frequency), they emit radio signal that can be captured by aerials or transformed into images.

Protons and neutrons have a property called spin or angular momentum which is a rotation around their own axis, having the protons also a magnetic moment which allows them to behave like a magnet. A magnetic moment, present in every proton, not only produces a magnetic field but also reacts to any other exterior magnetic field, so protons can be excited by powerful magnets producing a strong magnetic field changing the direction of the rotational axis.

Magnetic resonance imaging (MRI) uses a powerful magnetic field, radio frequency pulses and a computer to produce three dimensional detailed anatomical images being used to help the detection, diagnosis and monitoring of many conditions located in the chest, abdomen and pelvis.

It is a non-invasive exam, without any ionizing radiation being an advantage comparing to other tools, and it can produce detailed images of every kind of body structures: organs, soft tissues and bones.

To acquire this kind of exam, the patient lies inside a large cyllindrical magnet chamber and has to remain still to avoid blurring the images (Figure 2.4). The environment creates a strong magnet field (3000 to 6000 stronger than the field of the Earth). Often, an intravenous contrast agent is given to the patient to increase the brightness in the resulting images.

When the radio waves reach the patient, the protons of hydrogen present in the body are stimulated and spin out of their equilibrium, aligning with the magnetic field. Then, when the
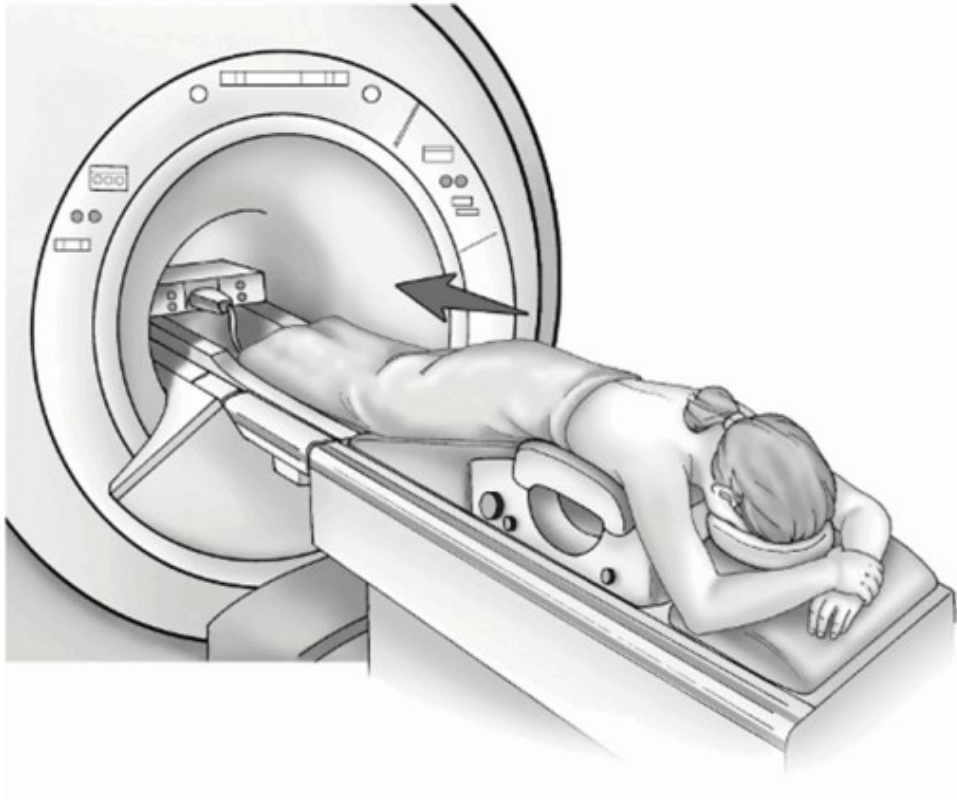
Figure 2.4: MRI acquisition representation [Reeve, 2018].

radio frequency is turned off, the sensors capture the energy released while the protons abruptly realign. The time taken to align with the magnetic field, the amount of energy released, and time spent to realign, called the relaxation time, depend on the environment and on chemical nature of the molecules, allowing to differentiate tissues by their magnetic properties.

Since the hydrogen has only a single proton it has the ability to produce the largest radio signal. It is an element very abundant in the human body, integrating the water molecule structure, it is the most suitable for the magnetic resonance image capture where the signal is produced by its magnetic moment after the realignment.

Tissues have different relaxation times, and the kind of acquisition is determined by the type of relaxation that is captured: T1 is the longitudinal one and T2 the transverse. This is what creates the images, being the relaxation times chosen the predominant source of contrast. T1-weighted images are the ones created by the longitudinal relaxation time acquisitions. They were chosen to be explored in this work since they are the most common technique used to chest MRI, providing better anatomic detail. They are characterized by the high magnetization from the tissues that have a lower relaxation time, being the brightest parts in the images. In this kind of acquisition, bones appear as dark parts, muscles with gray tones, bone marrow equal or brighter than muscles, fat with the brighter appearance and air is dark [Ken Saladin, 2003, Paul B, Adam M, 2007, Hage and Iwasaki, 2009].

MRI is a current method used to visualize numerous pathological lesions in hard tissues, such

as bones, showing complex structures which can lead to the presence of inadequate brightness and poor contrast in boundaries between hard and soft types of tissues [Gandhamal et al., 2017].

In long bones, like clavicle, the cortical bone thins out closer to the joints depending on the imaging process parameters, such as noise, bias fields and the partial volume effect. This makes the boundaries with other kind of bone and tissues more prone to be blurred, leading to segmentation issues and errors since none of the MR contrasts mode provide clear delineation (Figure 2.5) [Dam et al., 2015].
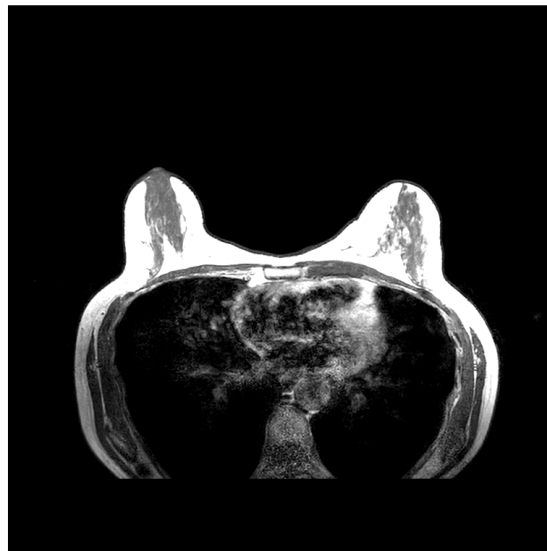
Figure 2.5: MR image example from an axial cut.

2.2 Segmentation Techniques

Today, there are many techniques already developed to segment bone parts in MRI but to the best of our knowledge, there are not techniques specifically to the bones of interest in this work: the sternum and the clavicles and for this particular acquisition setup.

Despite that, it is important to acknowledge the work already done and published in this field in order to understand which are the best candidate approaches to the achieve the aim of this work. For that, it will be taken in consideration the techniques that have already shown to produce relevant results.

2.2.1 MRI Bone Segmentation

There are some interesting approaches to general MRI bone segmentation, although not directly applicable, they allow extracting concrete information or segmenting a specific bone or body structure.

Hofmann et al. [2011] proposes a segmentation algorithm that combines image thresholds, Dixon fat–water segmentation, and component analysis to detect the lungs, in MRI from the whole body, acquired with patients with their arms up. The data preparation involves a low pass filter using a Gaussian kernel and morphological operations to eliminate information from the regions outside of the body of the patients. The segmentation itself includes a 5-class approach: air, lungs, fat tissue, fat and non-fat mixture and water where is applied a intensity based thresholding. Air and non-fat tissue were separated by thresholding the intensity-normalized in-phase images. Low intensity voxels were set as air with the help of a close operation to avoid misclassification. Fat and water voxels were separated based on Dixon images, being the fat characterized by having more than the double of the intensity value comparing to the water ones. The lungs were detectable as the largest connected group of low intensity voxels.

To segment bone parts present in MRI, Schmid et al. [2011], presented his approach which involves the use of statistical shape models (SSM). The process involves the creation of the SSM with a training set of shapes that resulted from images that were progressively segmented by a deforming template mesh guided by a radiologist. The statistics were inferred by this process. The initialization process attempts to find the best pair of rigid transform and shape parameters that minimize a cost function and its evolution is based on forces that are applied to these particles. The resulting discrete differential equations are solved by a stable Euler implicit numerical scheme. The external image forces appeal to go towards the desired boundaries by using image features, in order to isolate the desired objects.

To a semi-automatic approach, Ozdemir et al. [2017] described the use of the random forests classifier to train the model and a random walker algorithm to segment bone regions. It extracts statistical features from different orders using cubic patches of edge length centered at each voxel: the mean, the variance, the skewness and the kurtosis making a total of 12 features dimension. Also, the texture and curvature maps are extracted with the Gabor filters and anisotropic features to pronounce different orientation structures, especially in cancellous and cortical bone and their surrounding muscles. It is also referred the relevance of extracting context-integrating and location features in the proximity of the humerus since the shoulder has a dense constitution of muscles, tendons and fat. It incorporates contextual information of the spatial neighborhood and spatial shifts at multiple scales of different image maps. They were previously smoothed with a cubic kernel, to have relative orientation and distance-dependent information for each voxel that will help to characterize this kind of areas. For the segmentation, the random walker algorithm was chosen, being necessary to select the seed points and pairwise edge weights to perform the labelling to each voxel.

2.2.2 MRI Leg Bones segmentation

The majority work developed in the MRI bone segmentation field targets leg bones, such as the femur, the tibia and the patella.

Given the diversity of approaches already developed and reported, it is interesting to explore if any of those works use techniques that could be applied in the present work, or even if several techniques may be combined to produce better results.

In a paper by Gandhamal et al. [2017], beyond presenting their own approach for knee bone segmentation, a review on the existing techniques is made. This is shown in Table 2.1.

The main technique categories presented in the table are going to be explained and the ones with the most interesting contents are going to be described.

2.2.2.1   Semi-Automatic Techniques

Although semi-automatic algorithms may not be directly the intended approach for this work, they can contain some techniques that could be useful to understand the segmentation approaches already done.

A semi-automatic method is intended as a method in which in some phase of the process they require the use intervention. Usually, in this kind of approaches, the interaction occurs on the initial segmentation stage, to be chosen the starting points (seeds) on the regions of interest to give a reference for the segmentation initialization. This restriction leads to reliability issues, being a limitation of the performance of the algorithms, making them unsuitable for many purposes [Gandhamal et al., 2017].

Distribution and Texture-based active contours

From both methods presented in the compilation table the one proposed in Guo et al. [2011] has reported the best performance, evaluated using Dice Similarity Coefficient (DSC).

They present a hybrid active contour model in order to compensate the individual limitations of both methods that were fused: Geodesic active contours (GAC) model and histogram based Bhattacharyya gradient flow. The GAC model is an energy active contours model based on the classical snakes and uses the statistical overlap constrain to prevent method to the boundary's leakage, improving the image segmentation performance. The use of Bhattacharyya distance relates to the search for mismatched zones. It corresponds to boundaries between objects and background, such that were the distance value is bigger the greater is the probability that functions are different and correspond to a boundary.

Multiphase Chan-Vese model

In Jiang et al. [2008], an approach using the Chan-Vese model was proposed. It is a region-based deformable method for active contours based on energy minimization. It can detect objects whose boundaries are not necessarily well defined by the gradient but has the problem that can only isolate two scales of intensity of the image. To fight that, the Chan-Vese is used as the basal algorithm and then two improvements are performed. The multiphase Chan-Vese model is first applied and divides the images into two intensity regions, then, based on the type of intensity variance in the region, an area term is added to set the initial curves and regulate them. Finally,

Table 2.1: Review on Segmentation techniques for MRI leg images [Gandhamal et al., 2017].

Type	Key Segmentation Algorithms	Author, Year	Performance Metrics	Dependability
Semi-automatic	Distribution and Texture-based active contours	[Guo et al., 2011]	DSC- 0.94	*Depends on users for seed or contour initialization*
		Lorigo et al., 1998	DSC- 0.89	
	Multi-phase Chan-Vese Model	[Jiang et al., 2008]	not specified	
	Thresholding and Adaptative Region Growing, Bayesian Classification	[Dalvi et al., 2007]	(Femur) Sens.- 97.05, Spec.- 98.75 (Tibia) Sens.- 96.95, Spec.- 98.33	
		Lee et al., 2005	Not specified	
		Kapur et al., 1998	Not specified	
Fully-automatic	Multi-atlas registration and voxel classification	Tamez-Pena et al., 2016	(Femur) DSC – 0.95 (Tibia) DSC – 0.95	*Most algorithms depend on models, atlas designs and training dataset set for classification*
		[Dam et al., 2015]	DSC – 0.97	
		[Lee et al., 2014]	(Femur) AvgD–0.63 mm, RMSD–1.05 mm (Tibia) AvgD–0.53 mm, RMSD– 0.90 mm	
		Shan et al., 2014	(Femur)DSC – 0.96 (Tibia) DSC – 0.96	
	Graph Cut Algorithm	[Ababneh et al., 2011]	DSC – 0.95	
	Ray Casting technique	Dodin et al., 2011	(Femur) DSC – 0.94 (Tibia) DSC – 0.92	
	Random and Semantic Context Forests Learning	[Balsiger et al., 2015]	DSC– 0.92	
		Wang et al., 2013	(Femur) DSC – 0.94 (Tibia) DSC – 0.95 (Patella) DSC – 0.94	
	Active and Statistical Shape Models, Appearance Models	[Neogi et al., 2013]	Not specified	
		Bindernagel et al., 2011	(Femur) DSC – 0.94 (Tibia) DSC – 0.89	
		Seim et al., 2010	(Femur) AvgD – 1.02 mm, RMSD– 1.54mm (Tibia) AvgD – 0.84 mm, RMSD – 1.24 mm	
		Williams et al., 2010	(Surface)Seg. Err. – 0.648 (Volume)Seg. Err. – 0.431	
		[Fripp et al., 2007]	(Femur) DSC – 0.96 (Tibia) DSC – 0.96	
	Phase information for texture and feature based classification	[Bourgeat et al., 2007] [Bourgeat et al., 2006]	DSC – 0.87	

DSC - Dice Similarity Coefficient, Sens.- Sensitivity, Spec. – Specificity, AvgD. – Average Surface distance, RMSD – Root mean square distance, Seg. Err. – Mean Segmentation Error.

the re-initialization is removed meaning that the evolving curves will stay stable and close to the signed distance functions.

Thresholding, Adaptive Region Growing and Bayesian Classification

From the methods analyzed in this sector the work of Dalvi et al. [2007] is the most relevant, since it uses images from the T1-weighted multi contrast acquisitions. Despite not being exactly intended for this work, since in this acquisitions the bone structures have high intensities and it is a semi-automatic method, it showed to have a good performance.

The semi-automatic method proposed in Dalvi et al. [2007] starts with a noise reduction by using the curvature anisotropic diffusion filtering that prevents the edge information loss while improves the other parts of each image. Then, a Canny filter is applied to set the edge pixels to zero.

The segmentation starts with a rough threshold to separate high intensity pixels, where bone is supposed to be, from the lower ones. The bone class is morphologically eroded to ensure under segmentation and a seed must be manually added. The estimated area is then refined with a Laplacian level set segmentation.

2.2.2.2 Fully-Automatic Techniques

Multi-Atlas Registration and Voxel Classification

In Dam et al. [2015] it is combined rigid multi-atlas registration with voxel classification in a multi-structure setting, having the better result presented in this sector of techniques analyzed.

The registration step has the aim of producing a transformation from a given scan to a training space center. This allows the determination of the region of interest (ROI) for each anatomical part and transformation of scan features to a common feature space. This registration is a similarity transformation. The optimization of the method is achieved in two steps with Gaussian blurring of the scans firstly with a rough scale and then with a fine scale, as described in the Figure 2.6. With the resulting similarity transformations, the conversion to a training space center was defined as an element-wise median. When segmenting a new scan, it is registered to all training scans, without initialization, resulting in similarly transformations. The compositions of the new scan with the training space provide an estimation of the training space center via a training scan. Their element-wise median defined a robust estimate of the final multi-atlas transformation. The ROI is defined as the coordinate extrema encountered in the registered training scans giving a margin of 5% of the scan size in each direction, so the structures with margin for feature filter support are assuredly inside of the ROI. The features chosen for the voxel's classification were Gaussian derivatives up to order 3, nonlinear combinations of these such as the Hessian and structure tensor eigenvectors and values, intensity and position. The position and the Gaussian derivative features for a given scan were changed utilizing the similarity transform from voxels in a breadth-first manner until a connected component was formed. The number of seed voxels is set to ensure that all components of a suitable size are hit by a seed point applying sample-expand sparse classification

for the structures to be segmented. For each seed, the one versus all k-NN classifier resulted in classification strengths in the classified voxels and the ones not visited are set to -1 strength value. The structure-wise strength maps were combined to give origin to a single map of class labels by assigning each voxel to the structure with the highest strength.
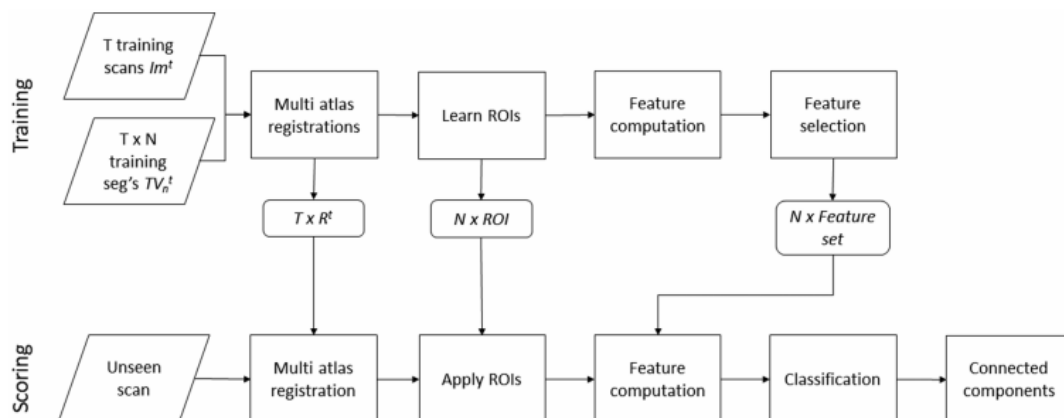
Figure 2.6: Dam et al. [2015] algorithm scheme

There is also a relevant technique to highlight in this sector, in Lee et al. [2014], since it is intended to be used in T1-weighted MRI despite having gradient echo and fat suppression.

So, Lee et al. [2014] proposed a segmentation based on three steps: multi-atlas building, locally weighted vote application (LWV) and region adjustment.

The multi-atlas phase includes intensity stretching, to set the intensities range, Gaussian blurring and after saving the similarity metric values the best matched atlases are selected.

LWV is used to merge the information from the obtained atlases and give origin to the initial segmentation result. Then, a Hessian matrix decomposition is applied to extract the unique intensity structure at a given local volumetric neighborhood. Being an Eigen decomposition, it produces three eigenvectors and eigenvalues to each voxel.

These eigenvectors represent the local orientation angles for each voxel and the eigenvalues give the magnitudes of the second-order derivatives along the orientation directions determined by the correspondent eigenvectors.

A Hessian-based analysis is also preformed using 3D Gaussian filtering which reduces noise and enhances the continuity in the local intensity fields. Then, the probability of correspondence between atlas voxels and the experimental ones and the correspondent LWV are calculated.

The statistical information, like means and standard deviation, allows to automatically determine seed points inside and outside bone regions for the graph-cut based method and the globally optimal segmentation is achieved with the max-flow-min-cut algorithm.

Graph Cut Algorithm

Ababneh et al. [2011] proposes a method that starts with image preprocessing, followed by a training data collection, to be used as reference for the block-wise feature extraction. It is followed by the application to classify images block to regions of interest (ROI) and background blocks.

The content of each block in the image is compared to representative training set constituted by blocks of ROI and background. The features used are empirically selected after showing a discrimination power. Then, a weight function is created combining sub-weights based on those features. The set chosen was the Grey-Level Co-occurrence Matrix (GLCM) derived features showing to be a good approach to separate bone from fat tissue. Once a new block is introduced its relevant features are extracted and saved, then it is determined which are most likely to be a ROI block trough high-likelihood. The blocks that did not show high similarity are compared to the blocks that were now selected as having high-likelihood to the training ones. The aim is to verify if the ones initially excluded as ROIs have similarities to the selected blocks, and if they have, they are considered as possible ROIs.

The ROIs and background blocks discovered are then used as seed points for the initialization of the graph construction. It is performed using a global cost function that uses regional and boundary weights and then applied a graph minimum-cut (GC) algorithm to generate the minimum cut mask image, a binary mask that represents all the segmented regions. This mask is subjected to a refinement based on its content, where the objects classified as background are filtered. To the remaining objects are applied morphological operations and leak detection to enhance the segmentation outcome.

The GC algorithm requires the construction of a source and sink (s-k) graph where each pixel is represented by a vertex in the graph and two terminal vertices are also added to the graph in order to represent the ROI and background respectively. The graph can be constructed creating an edge between each edge-pixel vertex and their four immediate neighbors being also an edge created between each pixel vertex and the terminal (s and k) vertices. A non-negative weight value is assigned to each edge and reflects the degree of the similarity between the two connected pixels. Each t-edge weight value assigned reflects the pixel similarity to both ROI and background. After the graph construction, the maximum-flow algorithm is applied to compute the GC that yields the optimal segmentation.

A specific regional cost function is utilized to measure the distance between each pixel value and the mean intensity of both ROI and background regions. The boundary cost function is obtained by the similarity measure between two pixels being the cost value inversely proportional to the dissimilarity between two pixels. A high penalty is paid in the GC when two very similar pixels are assigned to different regions.

The next phase is the refinement based on the content of the output from the GC algorithm since it does not always result in a clear segmentation. This happens due to the possibility of the lack of an exclusive set of seed points and due to the limited discriminative power of the cost function that defines the regional and boundary edges. This refinement includes the filtering out of the background and on the segmentation mask that contains a mix of ROI and background

segments. It is submitted to a Canny detector, since the edges are higher in fat tissues comparing to bone. There is also a leak detection, starting with an image opening and followed by a threshold segmentation to identify small elements that were segmented and are artifacts that do not belong to the ROI. Big segmented fragments are evaluated in order to discover if they belong to the ROI based on their edges content, intensity mean value and histogram distance. If the fragment is considered to be connected to bone objects they are preserved, if not, they are removed.

Random and Semantic Context Forests Learning

In Balsiger et al. [2015] it is proposed the use of Random forest (RF) voting, consisting the whole method in two main phases, as shown in Figure 2.7, the training and the segmentation.
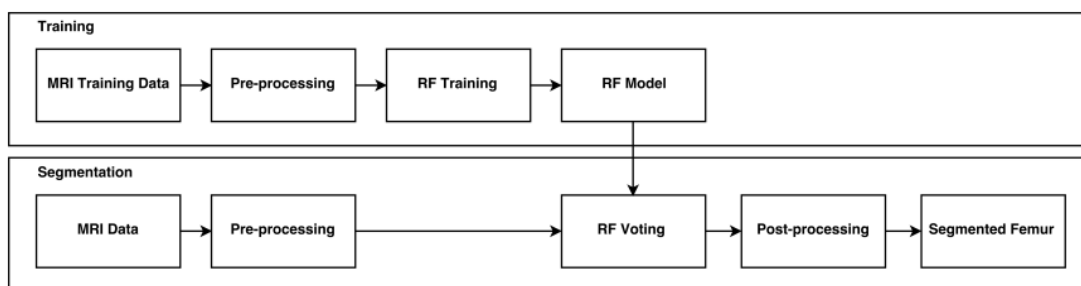
Figure 2.7: Balsiger et al. [2015] algorithm scheme

The preprocessing involves the use of z-score normalization to equalize the intensities and to remove noise a slice-wise Wiener filtering is applied, improving the signal-to-noise ratio (SNR) and also a slice-wise median. The z-score normalization is characterized as being very efficient, specially for Gaussian distributed data, but not very robust [Jain et al., 2005]. Then, the Wiener filtering is used to remove noise while it is kept as much as possible the signal characteristic features. To finish this phase, the application of a slice wise median filter improves the cohesion of the regions, preventing the excessive smoothing deriving from the previous steps.

The training phase relies on the extraction of features from the previously processed images followed by the RF classifier training with those images' voxels and their respectively labels. The set of of feature extracted is mainly statistical.

The first features are related to the spatial location, which is the relative position of each pixel in each slice. The distances are normalized and give the information of the approximately location to provide a standard measure. Then, volumetric features are calculated based on the 3D surroundings: the volumetric mean, volumetric variance and volumetric entropy. The next features are related to the data distribution, which implies the need of a sliding window, having the pixels whose feature is being extracted in the center.

The skewness, which is a measure of data asymmetry, in this case, calculates the symmetry that exists between the input pixel and it's the local neighborhood. The kurtosis is related to the tail of the data distribution. It measures the tail-heaviness, in this case, present in the local window. They both use the mean and the standard deviation of the neighborhood [McNeese, 2016].

Then, the Canny filter, an edge detector, is used in order to locate the edges in each slice, giving as the output a binary image where the pixels established as edges are positive and the others negative [Canny, 1986]. The last set of features extracted are the Hessian coefficients, calculated per slice.

The training itself is made using only 5% of the voxels labeled as bone and 5% labeled as non-bone by the ground-truth. The RF algorithm was built by bagging 20 decision trees to classify the pixels that were not in the training set.

The RF algorithm is a fusion of tree predictors, in the way that each tree depends on the values present in a random vector independently sampled in order to have the same distribution for all trees. The forests consist of using randomly selected combinations of inputs at each node to grow each tree to increase the result.

The bagging method choice is associated to the random feature selection. Each training set is designed, with replacement, from the original training set having the number of bags in account to the random feature selection. The use of bagging is taken as an enhancer of the accuracy when random features are used and it can be used to give progressing estimates of the error derived from the combined ensemble of trees [Breiman, 2001].

The post-processing step consists on morphological operations on classification previous results. Firstly, the binary image is eroded and it is extracted its largest connected volume. Then the holes are filled within areas and dilated in order to smooth the contour and eliminate artifacts that might be present at the borders of the segmented objects.

Active, Statistical and Appearance Shape Models

Neogi et al. [2013] published a method to segment the knee in MRI based on the shape prediction. With a set of training knees, it is applied active appearance models (AAMs): statistical shape model forms that learn from the objects in training sets based on their variation in shape and texture and encode them as principal components. Then, they are able to segment automatically MR images from the bones of interest using the matching of the characteristics that acquired from the training with the new images searching for the least squares sum of residuals. A second training set was used to identify vectors within shape space, able to discriminate the classes trough a linear discriminant analysis (LDA). This is a supervised form of learning that identifies a multidimensional function that separates the best the two classes reducing the shape dimensionality into a single scalar value representing the distance to the LDA vector for each portion of bone segmented. To train the LDA vectors, the images were searched using the AAMs and for each one, the values for the principal components were saved for each kind of bone knee (femur, tibia and patella). Then, they were combined and the LDA was performed with the principal components for each bone as input, with the examples already labeled. The dimension reduction is made, the bone shapes can be represented as principal components and projected in the LDA vector. The distance is then recorded and normalized.

The Fripp et al. [2007] approach uses a point distribution model (PDM) with the aim of representing the shape of bones and the variability among the database is modeled by 3D statistical

shape models. Then, a hybrid segmentation scheme based on 3D active shape model (ASM) is used to segment bones. This method reveled a high performance.

The individual statistics shape models (SSM) of each bone structure was obtained and they were combined using landmarks. Each structure gives origin to the whole knee SSM, providing the spatial relationship information.

The segmentation itself consists in SSM and matching criteria being performed in two steps. The deformation, where the position of each point is moved in 3D to best nearby match, and the shape restriction, where the pose and the shape parameters are estimated with the SSM help. The matching criteria is calculated finding the strongest gradient in the profile, satisfying the internal bone tissue constraint.

The segmentation is initialized through atlas and registration. The surface associated with the atlas propagates using an affine transform from registering the atlas to the image, SSM is used to estimate the pose and shape parameters of the surface in propagation being then utilized in the segmentation trough ASM. This method uses three-level multi-resolution Gaussian pyramid for the combined knee SSM and each image in the pyramid is smoothed along the sagittal plane with a median filter. The segmentation procedure is obtained using the Otsu method for an initial thresholding. Then, the bone intensity properties are estimated by their Gaussian distribution. Finally, the segmentation using the ASM method is applied, followed by a relaxation to the boundaries. It is achieved by a Laplacian operator and Humphrey's classes algorithm. After each iteration, the tissues previous parameters are updated using samples from the points with higher matching probability.

Phase information for feature and texture

Textural analysis has become a common way to perform segmentation of anatomical structures. One possible way to achieve to extract textural information is to submit images to different frequency subbands with different scales and then apply a filter and the features are extracted after those filter responses. In Bourgeat et al. [2007, 2006] it is proposed an automatic bone segmentation based on this textural information.

In this approach, the planes the images are considered in their coronal and sagittal plane where is expected that this kind of images have more textural information, especially in the sagittal plane.

The preprocessing step, the images are decomposed in their magnitude and phase components. The magnitude images are normalized in order to remain with a zero mean and a standard deviation of one, which is the effect of application of the z-score normalization [Jain et al., 2005].

Then, a bank of non-symmetric 2D Gabor filters is created with five different scales and six orientations as shown in the Image 2.8.

In the sagittal plane, where is expected to extract more textural information, the five scales of the Gabor filters were applied, but in the coronal plane only the first three scales where utilized, were it is expect to have less high frequency contents.

So, after the phase and magnitude extraction from the two planes, those images are subjected to the different Gabor filters. After that, to the magnitude of those responses it is applied a 3D
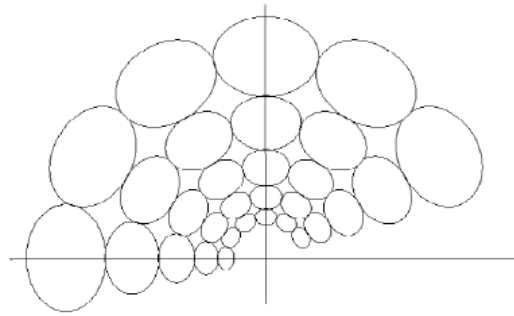
Figure 2.8: Bourgeat et al. [2006] representation of the Gabor bank filter.

Gaussian filter in order to smooth them. Then, the magnitude of those responses is summed across the slices to preserve the rotation invariance.

Applying the same bank of Gabor filters is expected to produce different results in phase and magnitude images and in their different planes, giving a large set of different features.

To the classification step, the authors used the Support Vector Machine (SVM) classifier with a Radial Basis Function (RBF) kernel [Suykens and Vandewalle, 1999].

Phase revealed to be a good discriminator between bones and surroundings, but not from the background. The magnitude revealed to be a good characteristic to separate bones from the background, but not from the other tissues. The combination of both sets of features produced the desired segmentation of bones from both kind of structures.

Distance Regularized Level Set Evolution

Lastly, the authors of Gandhamal et al. [2017] also present their own approach to the problem.

To provide better tissue contrast and to normalize the brightness present in knee MRI regions, a gray-level S-curve transformation is applied, which improves the gradient image magnitude, sharpening the edges between soft and hard tissues. Then, the contour initialization locations, that will be the seed points, are located through a 3D multi-edge overlapping technique. These will be used on the next step, the bone region extraction, by the distance regularized level set evolution (DRLSE). The region is expanded in the image, from the centered MR slice, what is considered as bone gives origin to a new centroid that is going to be used in the following slices. Then, the seed points are updated in each slice where the bone region is segmented.

For the post processing, the final regions extracted by the DRLSE algorithm are redefined in order to eliminate the outliers from the surrounding tissues in the regions due to over segmentation. The boundary displacement is identified by the point-to-point Euclidean distance between the region contours and the two consecutive slices and if it exceeds a certain threshold it is considered as leakage and it is adjusted. The boundaries are then smoothed by the Newton-Cotes method.

2.2.3   Chest Components Segmentation

Other works in the field of the chest components segmentation might give some glimpse on alternative approaches to segment the desired parts, since they consider the anatomical environment where the sternum and the clavicles are placed in the human body and all that surrounds them.

The aim in the work presented in Lu et al. [2006] is not for bone structure segmentation, although it is centered in the chest region MRI with the aim of isolating the breast, which is located in front of the sternum. The relevance of this work comes from the usage of the sternum as a pilot point to guide the breast segmentation, as shown in Figures 2.9.
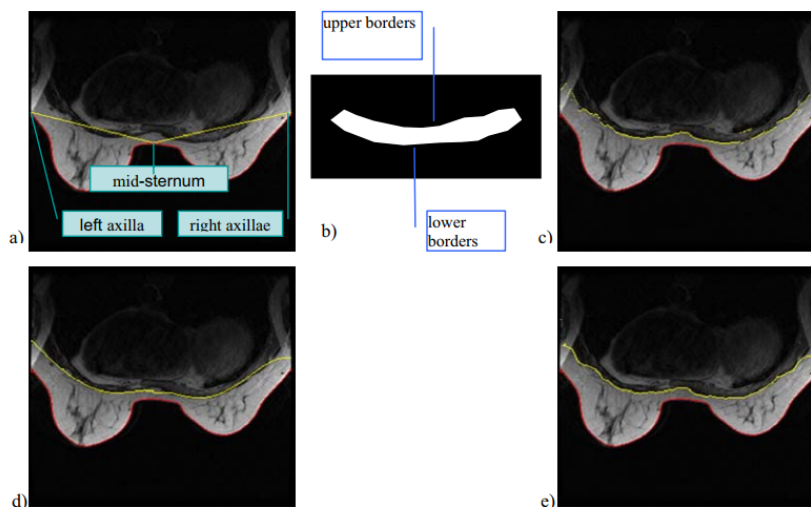
Figure 2.9: Lu et al. [2006] algorithm iteration demonstration from a) to e)

First, the breast-air boundary is located through region growing, using the Bernstein spline as the initial curve to the active contour model. Then, to locate the breast-chest boundary is used the previously obtained curve to identify the left and the right axilla. They are used as end points of the curve, being the mid-sternum the lowest point in the center of the curve. The three connected points make the initial boundary. Then, the muscle structure is searched through its gradient values, since it has lower densities, reflecting negative gradient in the upper border and positive in the lower one. The lower border points are refined into a smooth Bernstein spline and then with an active contour model.

Applied to breast images, Oliveira et al. [2012] detects breast contour and peak points. Despite working with images that contain depth information, which is the distance of each object to the camera, giving more information about its anatomical shape and relative position, the algorithm uses a threshold based on that depth information in order to exclude the background. After that, the contour detection phase begins. Since the breast boundary manifests as an accentuated gray-level intensity transition, between the breast itself and the rest of the body or background it gives origin to edges. In this way, if the image is interpreted as a graph in which every pixel is a node and edges connecting the adjacent pixels, applying an appropriate weight function, the contour

corresponds to a low-cost path through edge pixels. Being the breasts roughly circular shaped, the low-cost path is more easily achieved using polar coordinates. So, in the correspondent polar image each column represents the gradient during each radial line in the original image.

To get the intended minimum cost path, it is necessary to have a correspondent gradient polar image, which is the used as a weighted graph where pixels are considered as nodes and the edges are the connection between the neighborhood. Each pixel arc neighborhood consists on a weight calculated by an exponential law using the gradient of each two incident pixels. The minimum cost set of gradient pixels corresponds to the intended object, in this case the breast, contour (Figure 2.10).
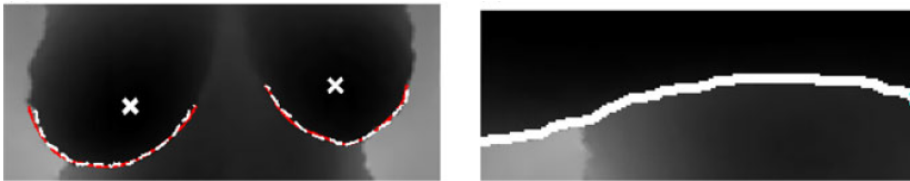
Figure 2.10: Oliveira et al. [2012] algorithm demonstration comparing the ground truth (solid red line) and the detected contour (dashed white line), zoomed on the right.

In Teixeira and Oliveira [2017] it is presented a detection algorithm to apply in T1-weight MR images using a minimum path approach using four main steps: thresholding for object selection, Region Growing segmentation over an entropy map, Convex Hull calculation to hone the previous results and to finish a minimum path algorithm is applied to achieve the intended result.

Initially, a first segmentation is made based on the intensity's histogram. This allows the elimination of the objects outside the profiles obtained through the algorithm iterations.

Then, the Region Growing is applied, based on an algorithm adaptation, requiring three inputs such as seed points, a 3D map, and inclusion criteria. The seed points were given by the previous step, being the objects eroded and thinned in a light way in order to generate contours. The 3D map was obtained using the probability of a voxel to belong to the object rather than the background based on its intensity. For the inclusion criteria, an eight-neighborhood connectivity and the mean and standard deviation of the intensities from the seed points are used.

The next step is the calculation of the Convex Hull, to refine the previous results due to the prevalent convex shape in artifacts located in the shoulder area.

The minimum path step is inspired in the Oliveira et al. [2014] but suffered some adaptations to this concrete application. The polar minimum path is described as behaving poorly with objects with small dimensions. The solution to overcome this problem was to bi-part the original processing, alternating between the sagittal to the axial plane in top slices and centroid of the previous slice segmentation serves as center to the new slice.

2.3 Summary

The techniques described have an important role in comprehending which approaches have already been applied in the field and their success.

It is evident that to the best of our knowledge there no examples of implementations for the intended objective in this thesis. Despite that, it is essential to learn what already had produced relevant results for solving segmentation problems in MR images even if they were created to segment other bones with different surrounding characteristics.

Most of the works described were made to be applied in leg bones which have different representation in MRI. This could mean that the implementation of these algorithms in the dissertation dataset may have to be adjusted to produce relevant results for the intended purpose.

The algorithms applied to segment chest components despite not having the same purpose, can be essential tools to achieve the intended objective, since they already are adjusted to the type of MRI acquisitions used in this work and deal with the components present in them.

Chapter 3

Methodology

3.1 Introduction

During this work, several approaches were tested in the available dataset in order to understand which one would lead the most satisfactory result. The implementation of the algorithms has been reproduced and developed in MATLAB which is the software chosen to execute the whole project, where this dissertation is inserted.

To achieve the main objective, the segmentation of sternum and clavicles structures in MRI, a few algorithms that worked in other conditions were tested in this context. It is expected, since we were exploring techniques used with another purpose, that they would not preform exactly in the same way in our work conditions and do not achieve the same results. Also, some adaptations or adjustments might be required. To start it is essential to recreate exactly how algorithms are described in the respectively literature, forming the baseline of the work.

Despite the large number of techniques mentioned in the Section 2.2.2 most of them did not seem appropriate for this work purpose, due to the type of MRI acquisitions used or even the type of approach they use to reach their aims. The approaches that seemed more relevant to initially reproduce used classification techniques were the Bourgeat et al. [2007] and the Balsiger et al. [2015], both use feature extraction, meaning that different set of features and types of classification methods were tried. In addition, another algorithm, inspired in Oliveira et al. [2012] and Teixeira and Oliveira [2017] was developed. Firstly, it is defined the ROI, where the objects are estimated to be in, then the slices are elliptical transformed and the gradient of each image is weighted in order to set the low cost pixel path as the object contours.

In the following Sections the pipelines of the algorithms above mentioned will be given in detail, starting with the classification methods and then to the gradient based segmentation, where the approaches for the sternum and clavicles are individualized and will be properly explained.

3.2   Feature Extraction and Classification Based Methods

The classification methods based on feature extractions demand an initial definition of sets, the training and the test set, in order to develop a model that fits properly the data given as positive. The aim is to identify as object of interest and discard data given as being of no interest. To achieve that, the training set has to be annotated, to identify the pixels of interest, and just after that the preprocessing and features extraction is performed. It allows to take into consideration both kinds of data, to cross validate and train the model properly with both kinds of examples (Figure 3.1).
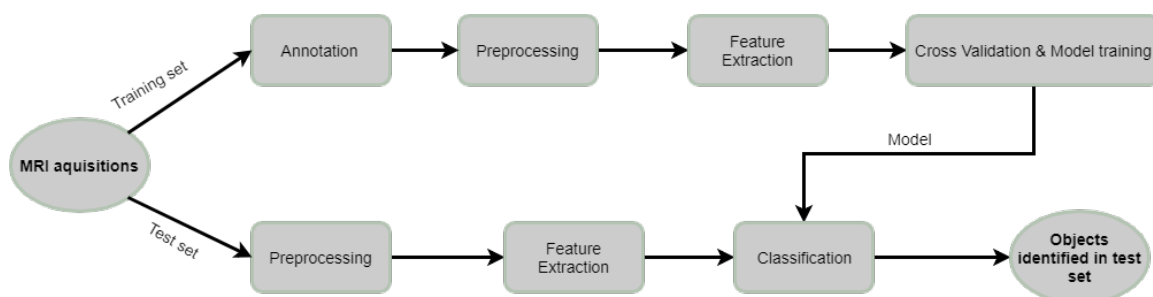
Figure 3.1: General Feature extraction and Classification methods pipeline.

Having a model adjusted to the training set, it is possible to classify the new pixels, from the test set, after they are being preprocessed in the same way and then extract their features. The model evaluates the features belonging to each pixel and then classifies it as object of interest or not.

In this case, two different classification methods were applied to two different set of features, providing from different algorithms. Their performance was evaluated in order to realize if any of them could constitute the desired solution for the bone identification problem.

Textural features method

Firstly, the Bourgeat et al. [2007] algorithm, which was designed in order to obtain segmentation results in knee MR raw images, achieves it extracting textural information from the sagittal and coronal planes, as explained in the previous chapter in Section 2.2.2.2, with good performance measure and quite applicable to the chest imaging context.

This method uses the magnitude and the phase components of each image which are characterized by the following relation with the original image (I) (equation 3.1):

$$I(x,y,z) = A(x,y,z) \times e^{j\varphi}(x,y,z) \tag{3.1}$$

Where A(x,y,z) is the magnitude and $e^{j\varphi}$(x,y,z) is the phase portion, representing different information about image intensities transitions. The magnitude quantifies those transitions and the phase represents their direction (Figures 3.2a, 3.2b).

(a) (b)

Figure 3.2: Magnitude (a) and phase (b) representations of chest MRI in axial cut.

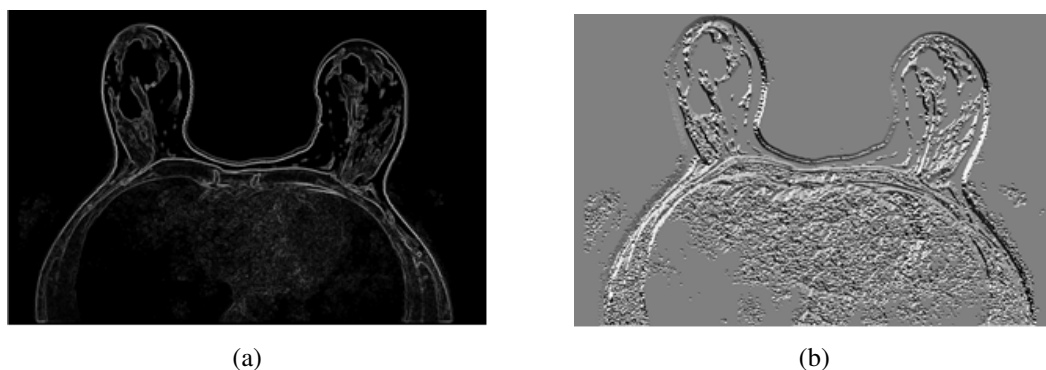The preprocessing step consists on the intensity's normalization of the magnitude, using the z-score method [Jain et al., 2005] which is calculated using the arithmetic mean (μ) and standard deviation (σ) of the data. In this case the intensities of pixels (Equation 3.2):

$$s_k\prime = \frac{s_k - \mu}{\sigma} \tag{3.2}$$

The output ($s_{k'}$) is obtained based on the input (s_k) distribution. The resultant set of magnitude and phase images extracted from sagittal and coronal planes are subjected to different Gabor filters which frequencies and scale influence its effect on images. The results of every filtering frequency rotation are summed across the acquisitions slices in order to produce features dependent on frequency cycles but rotation invariant. The five pixel frequency scales and six rotations, from the original algorithm, were maintained in a first approach and then also smaller cycles scales were also used to produce different Gabor filters, in order to evaluate if the results would increase the final results.

The resultant features per MRI slice are:

- Magnitude;

- Magnitude after Gabor filtering in every rotation and summed all the responses (one per scale);

- Magnitude after 3D Gaussian filtering the previous Gabor filtering (one per scale);

- Phase;

- Phase after Gabor filtering on every rotation and summed all the responses (one per scale).

The correspondent features of each randomly sampled pixel are passed to the modeling and cross-validation step, serving as guiding examples for the classification model adjustment. Several sample sizes were tried in order to optimize the method, maintaining the number of objects of interest and non-interest pixels extracted equal and homogeneously distributed per object containing slice.

The classifier originally used was the SVM, with a RBF kernel [Suykens and Vandewalle, 1999]. The cross validation was performed with different fold values, in order to optimize the parameters to the segmentation contexts.

The RF classifier [Breiman, 2001] was also applied to the same features, with the purpose of testing another approach, in this case, a classification that combines groups of the given features and analyses which shows to be the best sub-set of features to learn the object characteristics. Varying the number of bags and the cross-validation folds, this method was also optimized.

Statistical, location and edge features

The Random Forest classifier was applied to the previous described features and being the classification method used in one of the previously described algorithms in Chapter 2 as successful in leg bone segmentation, the Balsiger et al. [2015] was followed and its feature approach was used, setting another possible solution for this work.

For the preprocessing phase, Balsiger et al. [2015] uses the z-score normalization, previously described, as the first step, relying on the mean and standard deviation [Jain et al., 2005].

The second step is to apply the Wiener filtering. It uses the minimum mean squared error (MSE), assuming the input images as two components, the free-noise image plus the additive Gaussian noise, to obtain the estimation of the free-noise image, the desired output. It works in optimal conditions when the input (free-noise image and its noise) are stationary Gaussian processes. The method has in consideration the local values of mean and standard deviation, smoothing less where the variance is higher which contributes to preserve important characteristics of the original image [Jin et al., 2003].

The last preprocessing step is the application of a slice wise median filter consolidating the previous ones, resulting in images as the one represented in Figure 3.3.

Figure 3.3: Balsiger et al. [2015] preprocessing on MRI chest acquisitions.

Then, the feature extraction begins, using some volumetric and slice information. They are statistcal, edges and location based features.

The volumetric mean (μ) , volumetric variance (σ) and volumetric entropy (E) have in consideration the input pixel (v) and its location in each axis (i, j, k):

$$\mu = \frac{1}{N} \sum_{i=\frac{-I}{2}}^{\frac{I}{2}} \sum_{j=\frac{-J}{2}}^{\frac{J}{2}} \sum_{k=\frac{-K}{2}}^{\frac{K}{2}} (v_{i,j,k}) \tag{3.3}$$

$$\sigma^2 = \frac{1}{N} \sum_{i=\frac{-I}{2}}^{\frac{I}{2}} \sum_{j=\frac{-J}{2}}^{\frac{J}{2}} \sum_{k=\frac{-K}{2}}^{\frac{K}{2}} (v_{i,j,k} - \mu)^2 \tag{3.4}$$

where N= I . J . K

$$E = - \sum_{i=\frac{-I}{2}}^{\frac{I}{2}} \sum_{j=\frac{-J}{2}}^{\frac{J}{2}} \sum_{k=\frac{-K}{2}}^{\frac{K}{2}} p(v_{i,j,k}) \, log(p(v_{i,j,k})) \tag{3.5}$$

The statistical slice measures, skewness (s) and kurtosis (k) use the mean and the standard deviation, but in this case in the slice neighborhood:

$$s = \frac{E(v - \mu)^3}{\sigma^3} \tag{3.6}$$

$$k = \frac{E(v - \mu)^4}{\sigma^4} \tag{3.7}$$

The last features are also related to each slice and are the Canny filter [Canny, 1986] application and the Hessian matrix (M):

$$M = \begin{bmatrix} \frac{\delta^2 I}{\delta x^2} & \frac{\delta^2 I}{\delta x \delta y} \\ \frac{\delta^2 I}{\delta y \delta x} & \frac{\delta^2 I}{\delta y^2} \end{bmatrix} \tag{3.8}$$

To summarize, the new set of features extracted are the following ones:

- Normalized spatial location (x,y,z);

- Volumetric mean;

- Volumetric variance;

- Volumetric entropy;

- Skewness;

- Kurtosis;

- Canny filter distance;

- Hessian matrix coefficients.

The RF classification was tried and optimized the number of bags and cross-validation folds. Also the SVM classifier applied to this new set of features in order to evaluate its performance and if any of them constituted a valid solution for the main problem.

3.3   Gradient Based Segmentation

A completely different approach was developed based on Oliveira et al. [2012] and Teixeira and Oliveira [2017], algorithms that produced relevant results in more similar contexts: breast contour detection and MRI T1-weighted artifact detection on chest acquisitions respectively.

Being the edges of these objects often differentiated from the surroundings, but not their interior, the object contour detection as a first output must be another perspective to consider as possible manner to accomplish the desired solutions.

In Figure 3.4 it is outlined the main steps taken to reach the object segmentation, from the MRI acquisition volumes as the input, to the object contours which are the algorithm main output.
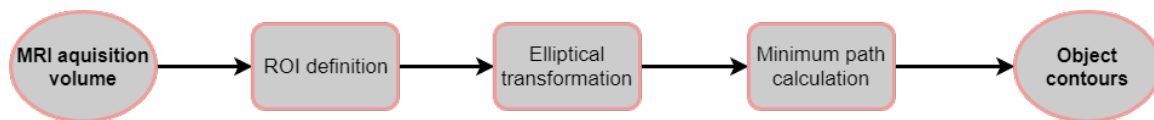

Figure 3.4: Gradient based segmentation method pipeline.

The first step is to restrict the segmentation to an area were the objects are certainly contained in, discarding the other parts of the acquisitions, defining in that way a ROI.

Having the sternum and the clavicles an approximately elliptical and round rough shapes, seen by the axial plane in MRI, the image transformation of the images is a step to take in the process to empower the next step. Transforming each slice ROI in order to open the object contour and highlight it is the main objective of this stage. Being elliptically modified, the transformed images provide the path calculation from one margin to another, once the object was opened and stretched.

Through the minimum cost path calculation, applying the Oliveira et al. [2012], Teixeira and Oliveira [2017] approach to identify the object contours, based on the gradient transformed images, the final step is achieved.

In order to overcome some possible sternum segmentation problems, a post-processing phase follows the previous mentioned steps. It also provides the estimation of the clavicle content number of slices in each acquisition.

Minimum Path approach

The minimum path algorithm, to reach object contours, follows the main explanation explicit in Chapter 2 from Oliveira et al. [2012]. It requires the calculation of the desired minimum path through gradient images in which gray-level transitions are accentuated and quantified in magnitude gradient representations.

The sternum and clavicle contours are darker than the surroundings, being highlighted in those kind of representations, to be identified by this method.

The gradient images are treated as a graph, having the pixels as nodes and edges connecting to the adjacent pixels. The aim is to evaluate which pixel combination gives origin to the path with minimum cost. In this case, it will be the bone contours.

The path cost (f) weight of each eight-neighbor gradient pixel arc (g) takes into account the exponential law described in the Equation 3.9.

$$f(g) = f_l + (f_h - f_l) \ \frac{exp(\beta \, (max - g)) - 1}{exp(\beta \, max) - 1} \ \ where \ f_l, f_h, \beta, max \in \mathbf{R} \qquad (3.9)$$

Being f_l=2, f_h=126 and β=0.025 fixed constant values, set to optimized the minimum cost calculation in MR images in Teixeira and Oliveira [2017], and having the input scaled to $[0, 255]$. The path stated as minimum is the group of successive pixels whose weight is the lowest, meaning their crossing represents the smaller cost.

The following sections will describe the higher details of each method stated. The detailed pipelines for sternum and clavicles segmentations are presented in Figures 3.5 and 3.6. The main differences are in the ROI definition, since there are two clavicles, two ROIs need to be established, one right and one left. The identification of the objects, following the ROI detection, varies between the two types of objects. In sternum an intensity threshold method is used, unlike in clavicles which an edge detector is applied.
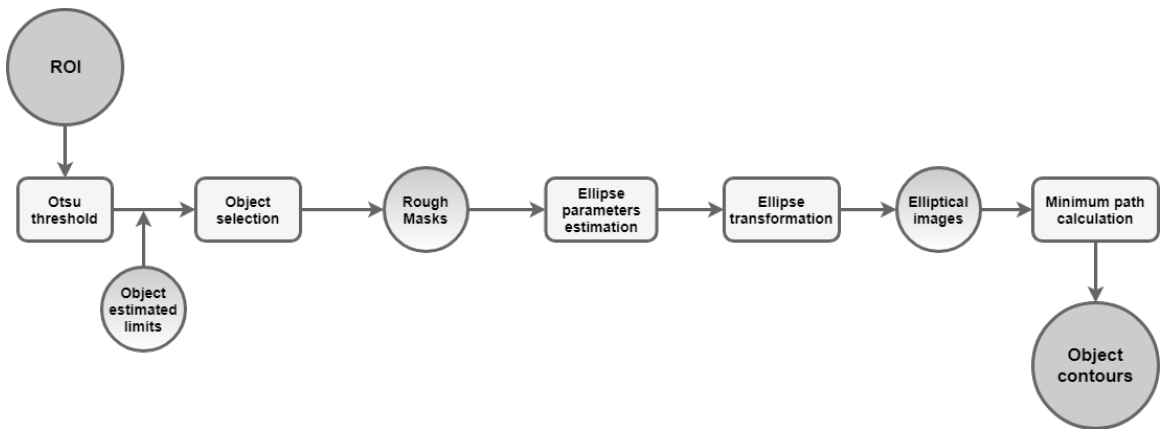
Figure 3.5: Sternum segmentation detailed pipeline.

The steps taken in each one of the cases are going to be disclosed in the following sections.

3.3.0.1 ROI Definition

It is important to identify the central part of the slices, discarding the background and other types of tissues, specially breast fat tissue which is widely present in central slices. The rejection of the surrounding irrelevant parts allows to sharpen the area of interest. As mentioned before, the sternum is a single bone unlike the clavicles. This implies the establishment of two ROIs, one for the right and other for the left side. Therefore, this stage has differences between the two types of bones and they will be presented individually.
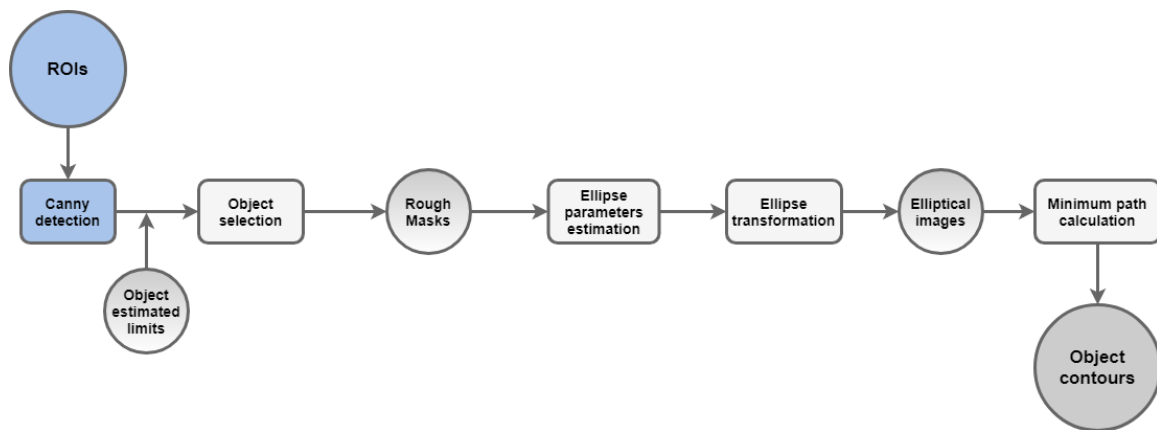
Figure 3.6: Clavicles detection detailed pipeline.

Sternum

The sternum, when visualized in a T1-weight MRI chest acquisitions, typically sectioned in the axial cut, it is one of the central components of the acquisition slices (Figure 3.7).
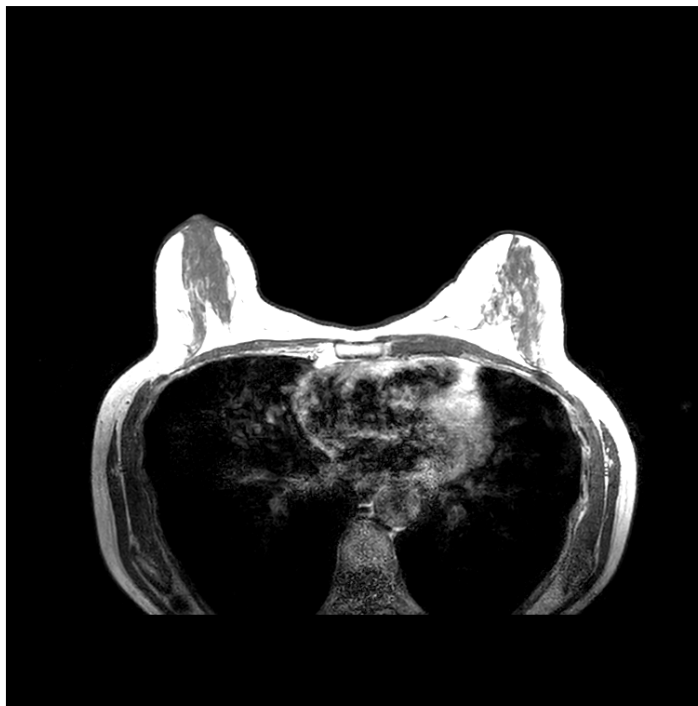
Figure 3.7: MR slice in the axial cut.

The rejection of the unwanted areas is firstly achieved using a 2D snake [Caselles et al., 1997] in the upper and lower slices, where the breasts are not the most anterior parts. Being the background constituted by very low intensities, mainly zero values, there is an accentuated gray-level transition. The edges between the patient body and the background itself are easily separated.

Applying a Otsu threshold [Otsu, 1979], to the original acquisition, it is possible to roughly distinguish sternum limits and also locate the breast adipose tissue in the anterior chest area, as shown in Figure 3.8.

Figure 3.8: Otsu threshold with sternum roughly defined limits in the center axial view.

Considering that the sternum is contained between the two breast peaks, since it is located in the middle of the chest, their identification serves as lateral reference to the ROI limitation.

With this rough Otsu mask, dividing it equally into right and left side, it is possible to identify the two most anterior high intensity transitions. They are identified as the breast peaks and both ROI lateral limits are established.

The sagittal view of the anterior portion of the acquisitions is the next content to be explored (Figure 3.9a). The sternum is the middle-intensity object limited by the high to low intensities transition in the anterior area. Calculating two vertical minimum paths, using the method previously described, in this most anterior chest area (guided by the high intensities transitions which empower the low cost for the intended limits) it is possible to get an estimated position of the sternum anterior and posterior limits in each slice.

(a)   (b)

Figure 3.9: Sagittal view of the sternum (a) and its correspondent gradient image (b).

Firstly, the most anterior limits are the target, which are the easiest to be detected due to the high intensity fat tissue proximity. Identifying the abrupt fat tissue-sternum intensity transition, using the central 10% profiles allows the establishment of two starting points for minimum cost paths (Figure 3.10). The resultant paths correspond to the upper and lower anterior sagittal sternum limits.
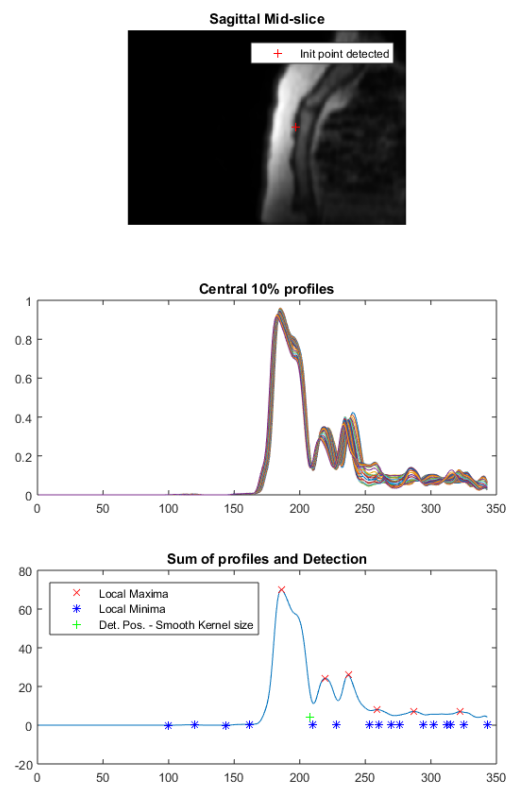

Figure 3.10: Initial point definition based on central profiles representation.

The posterior limits are estimated after excluding the anterior portion previously detected. In the same way as the anterior path was obtained, the two posterior paths give origin to the estimation of the sternum sagittal posterior boundaries.

Having the anterior and posterior detected limits of the intended object and a lateral restriction it is important to carry out a reduction of the image information in order to focus the procedures on the region of interest to hone the desired segmentation (Figure 3.11).

Being the sternum a bone in a curved shape, seen in the sagittal plane (as shown in Figure 3.9a), not only its shape changes along the slices, but also its relative position in the image across slices. To avoid that and in order to improve the reproducibility of the algorithm procedures, an alignment is preformed taking in consideration the anterior positions detected through the acquisition.

The maximum difference between correspondent anterior and posterior positions, considering the irregular shapes and size of the sternum representation on each slice, is taken as a posterior limit to shape the ROI. This is done to avoid the elimination of any relevant part of the image for the intended segmentation.
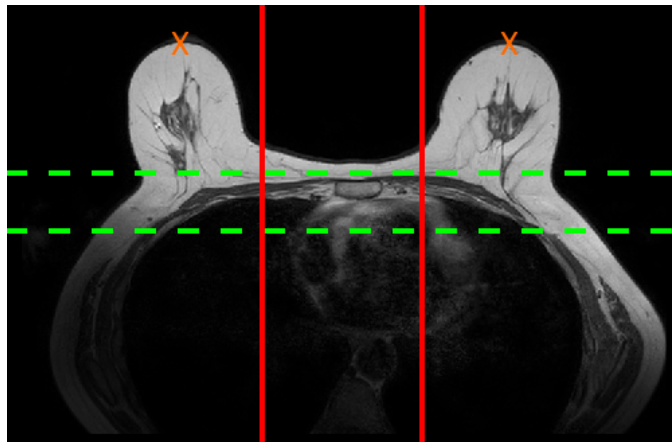
Figure 3.11: ROI limits representation.

Figure 3.12: ROI example.

Having the ROI defined (Figures 3.11, 3.12) it is possible now to proceed to the next main step in this gradient based method for the sternum detection.

Clavicles

The clavicles articulate on upper part of the sternum manubrium (Figure 3.13). This provides the possibility of using the identified sternum upper slices ROIs as reference.

Figure 3.13: MR image containing clavicles.

The method to achieve the ROI was maintained, since the clavicles are also close to the sternum but the lateral limits, referenced by the breast peaks, were slightly increased. This was made to ensure that there were not discarded objects, despite the clavicles not being most of the times totally represented in the MRI chest acquisitions. The anterior tolerance has also to be increased, as the clavicles are in a slightly more anterior position. A tolerance of 10% was chosen for both cases.

This new main ROI is divided taking the sternum middle as reference and next process steps are doubled in order to identify the clavicles in the two image sets: the left and the right side clavicle ROIs (Figures 3.14a, 3.14b).
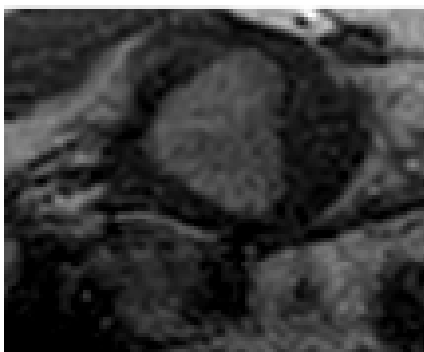
(a)   (b)

Figure 3.14: ROI clavicles examples from left (a) and (b) right side.

Having the clavicles ROIs also defined, it is possible to carry out the next main step: the elliptical transformation.

3.3.0.2 Elliptical Transformation

Sternum shape detection

Applying another Otsu threshold based mask, but now created in new ROI images and knowing the sternum relative anterior and posterior position, rough shape masks are created (Figures 3.15a, 3.15b).

(a)   (b)

Figure 3.15: Sternum shapes detected after object selection (a) and the correspondent content (b).

Based on the segmentation and the object selection is made using the estimated position, contained between the previously estimated anterior and posterior limits.

The detected shape of the sternum in each slice is now represented in masks, which will allow the adapted elliptical transformation.

Clavicles shape detection

Differently than on the sternum shape identification process, this step uses a Canny filter [Canny, 1986]. The purpose is to obtain an initial segmentation on the ROIs highlighting the possible boundaries of the clavicles (Figures 3.16a and 3.16b). Having more than the intended contours identified, it is necessary to select the objects whose contours were identified in order to remain only with the relevant ones. After filling the closed detected edges, their area and centroid were the properties chosen to be used as a selection criteria. Relating the previously identified anterior and posterior limits, as the clavicles articulate and surround the sternum.

The object resultant from the Canny edge identification is selected by its centroid smallest distance to the sternum and having the biggest area, being stated as a clavicle rough mask (Figures 3.17a and 3.17b). This will provide the estimation of the elliptical transformation parameters to be adjusted.

(a)   (b)
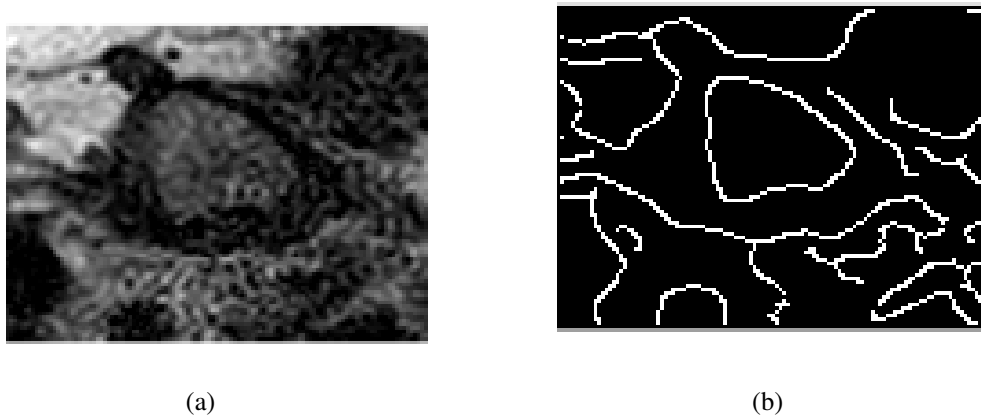
Figure 3.16: ROI clavicle representation (a) and the correspondent Canny filter application (b).

(a)   (b)

Figure 3.17: Detected objects after Canny edges filling (a) and correspondent clavicle selection (b).

Elliptical parameters estimation

With this new and more restricted binary images, it is possible to estimate the object elliptical parameters. To execute the image transformations, adapted to each slice content characteristics. This allows the correspondent gradient image to provide a better response to the minimum path search.

As previously referred, the segmentation through the Otsu threshold and the Canny detection are not very precise and the intensities vary between slices. It depends on the sternum intensities present in each slice and what surrounds it. It is expected that not every slice will contain an object after the threshold segmentation and object selection.

Firstly, where there is an object, it is estimated for each slice object the correspondent elliptical parameters. It is achieved by the best elliptical fit, given the object points. In this case the shape mask, evaluated by the Least square, which is the minimization of the squared fitting residuals sum [Hendel, 2008, Suykens and Vandewalle, 1999].

Taking the quadratic curve of an ellipse as the fitting objective (Equation 3.10):

$$ax^2 + 2bxy + cy^2 + 2dx + 2fy + g = 0 \tag{3.10}$$

It is necessary to find the constant values a, b, c, d, f, g, that best minimize the residuals in the least square sense, but the elliptical description can be simplified into:

$$\frac{(x-x_0)^2}{a^2} + \frac{(y-y_0)^2}{b^2} = 1 \tag{3.11}$$

Where

$$x = a\cos(\psi) \tag{3.12}$$

$$y = b\sin(\psi) \tag{3.13}$$

To illustrate this elliptical description, in Figure 3.18 it is represented the importance of each parameter to be estimate. It demonstrates where each elliptical variable is going to be applied in the image transformation.
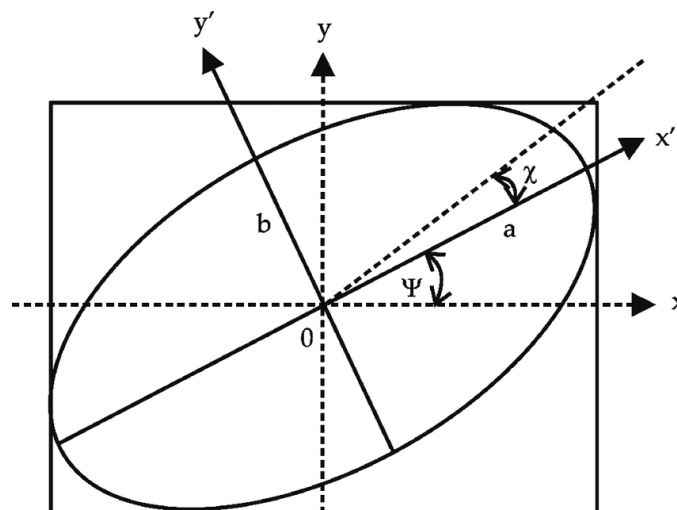

Figure 3.18: Ellipse representation [Therézio et al., 2017].

For each image it is necessary to obtain the following estimations:

- Semi-major axis (a)

- Semi-minor axis (b)

- Center coordinate in xx axis (X_0)

- Center coordinate in yy axis (Y_0)

- Angle of rotation (ψ)

The transformation of each pixel (x,y) can be performed based on these values [Hendel, 2008, Weisstein, 2018, Therézio et al., 2017].

Following this estimation parameters criteria, the slices in which the sternum was not identified in the primary threshold, have to be estimated to perform the image transformation.

For those missing slices which are in between already estimated slices, their parameters can be interpolated. This is achieved considering the upper and lower neighbors, weighting their parameters according to the distance to the slice to be interpolated, giving more importance to the near ones which are expected to be more alike.

The weight given to each previously estimated parameters, that surround the missing one, has in consideration the relative position of the slices used to interpolate, following the Equation 3.14:

$$weight = \frac{n}{N+1} \qquad (3.14)$$

Where n is the distance to the slice to be interpolated and N is the number of missing parameters between the slices with parameters already estimated (gap).

For the boundary slices, meaning the missing shape masks in the upper and lowest acquisition slices, their parameters must be extrapolated. It is achieved based on the closest ones whose parameters are known. This calculation is also weighted according to the distance to the missing parameters slice. The already extrapolated ones serve as reference to the following, until the limiting upper or lowest slice have their own parameters.

Following the same strategy, the parameters are being estimated from the inside out in order to follow the guidance of the values already established, weighting them gradually according to the distance between the slices.

Having every slice elliptical parameters estimated, the ROIs, that were in Cartesian coordinates (x,y) are transformed into elliptical (x_e,y_e) (Equations 3.15 and 3.16), following the previous presented Equations 3.11 to 3.13:

$$x_e = X_0 + x\cos(\psi) - y\sin(\psi); \qquad (3.15)$$

$$y_e = Y_0 + x\sin(\psi) + y\cos(\psi); \qquad (3.16)$$

This transformation is performed in every slice and will provide the accomplishment of the following main step. Two examples of the coordinate transformation are represented in Figures 3.19a - 3.20b.
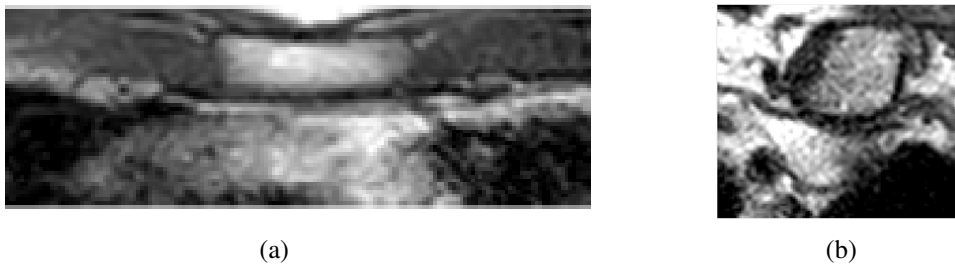
(a)

(b)

Figure 3.19: Two different sternum ROI examples.

(a)

(b)

Figure 3.20: Correspondent two elliptical transformation examples.

3.3.1 Minimum path calculation

After the elliptical transformation, from the last pipeline step, the gradient magnitude of each image is fundamental to achieve the desired results. In this kind of images, the edges of the objects are empathized since they represent high intensity level transitions, and having the object contours darker than the surroundings. They are identified by those representations. The transformation by the exponential law previously mentioned (Equation 3.9), makes the predominant edges to get values close to zero, meaning that the minimum path should correspond to the intended contours.

Not having a specific starting and ending point every possible path cost is evaluated from one margin to the other in the gradient elliptical image. When reverted to the Cartesian coordinates there is the possibility of not corresponding to a closed contour, starting and ending in the same point. So, to overcome this, the two resultant start and ending points from this first iteration are considered to be the staring and the ending point in other two minimum path cost iterations (Figure 3.21). Also, the original gradient image is rotated in 180° to ensure that the margin-to-margin iteration points, corresponding to the minimum cost, are the same. If they are not, two new point-to-point iterations will be made, being those points the start and ending reference (Figure 3.21).
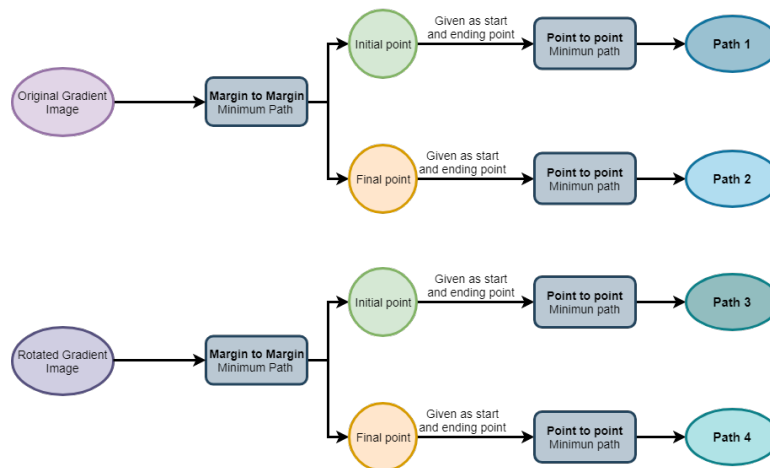
Figure 3.21: Minimum paths pipeline.

Having four possible paths to be the object desired contour, the criteria must be maintained, and the four global costs are compared and the path with lowest cost is the selected as the object contour.

The minimum cost path should correspond to the objects limits in the original ROI image, being necessary to undo the coordinates transformation, which will lead to the contour in the Cartesian coordinates system.

3.3.2 Post-processing

As the elliptical transformation parameters is estimated for every slice, means that a correspondent minimum cost path is obtained. So, even in the images that the bones are not present there is a contour limiting something.

To overcome this expected over-segmentation, the sternum profile is evaluated, in order to identify which slices are more prone to contain the desires objects. This is achieved using a Region growing [Mehnert and Jackway, 1997] (RG) based algorithm applied to the coronal compressed view of the sternum (Figure 3.22), where the number of slices in the acquisition is the number of width pixels .

Figure 3.22: Sternum compressed coronal view.

The required seed points to implement the algorithm are estimated based on the sternum intensities profile. The sternum i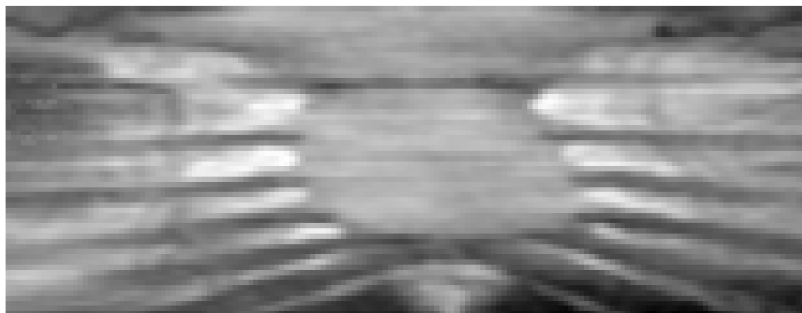s an irregular shaped bone having, most of the times, an abrupt transition between the manubrium and the body components (Figure 3.22). To overcome this recurrent event, it is required to properly estimate seed points, through the identification of the components transition area. An intensity profile is made along the central area (10%), to evaluate if there is a relevant derivative transition along this profile. If present, two central seed point are given to the RG in order to properly identify the upper and lower sternum slices, as represented in Figure 3.23.
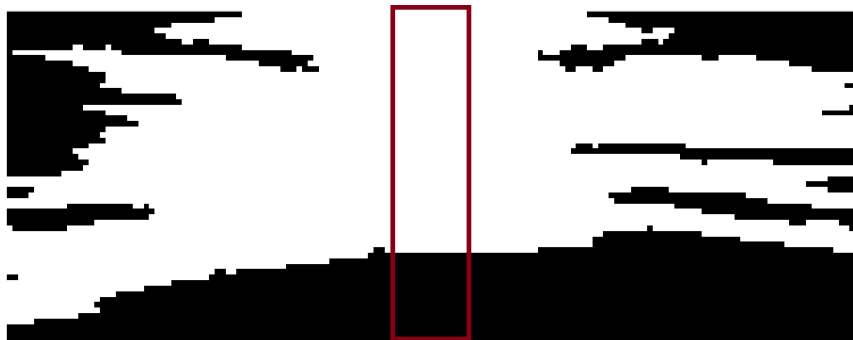
Figure 3.23: RG coronal mask to identify the sternum content slices.

The same central area serves as reference to the identification of the sternum content relevant slices, providing the segmentation refinement.

This identification process is also used for the clavicle identification. The number of slices where they can be present directly depends on the upper sternum limit. If the sternum is detected to appear in the initial slices, less clavicles content slices will be present. If instead, the sternum is only detected in lower slices, clavicles should be widely represented. Therefore, considering the possibility of sternum and clavicles coexistence in some slices, as they articulate, the upper limit detected of the sternum is considered as clavicle content and also the immediately lower slice.

Having identified the contours of the object in proper slices, this segmentation process is taken as finished after the filling of the contour limited area, creating binary slices where the intended bones are identified.

Chapter 4

Results and Discussion

4.1 Dataset

The dataset consisted in 14 (fourteen) MRI acquisitions from different breast cancer patients, in the initial phase of the treatment, collected with patients with their arms up. Each acquisition has a set of 60 (sixty) images corresponding to axial slices of the chest patient area. Usually it captures the shoulder area, from the clavicles, until the middle of the ribs (after the end of sternum).

Firstly, the dataset was divided into a set of training and test groups, in order to obtain and statistically compare each method results as most of them required training for the classification of images.

From the 14 acquisitions with correspondent annotations, 10 (ten) were randomly set for training and 4 (four) as test.

The annotation consists in the creation of a mask for each acquisition where the pixels of the sternum or the clavicles are identified as positives and the rest, the parts of the images that are not of interest, are stated as zeros. This produces logical acquisitions masks indicating which pixels should be classified as sternum or clavicles.

To achieve that, each one of the slices has to be evaluated as a single one but also in the context, related with the slices above and below in order to make a consistent annotation and not compromise the results.

The annotations in the training phase are used as ground truth to the classifiers modeling. In the test phase, they provide the comparison of the results from the algorithm tested and the results that were desired (the annotation). Ideally, they would be the same.

4.2 Results

This section contains the statistical results from the previously detailed algorithms that were applied to the referred dataset.

The methods used to statistically evaluate the performance of the algorithms used to solve the main problem were: Accuracy, Precision, Recall and DSC.

This metrics are calculated based on four types of pixel classification. The True Positives (TP) and False Positives (FP) are the number of correct and incorrect classified as pixels of interest, and the True Negatives (TN) and False Negatives (FN) are the number of correct and incorrect pixels stated as non-interest. The sum of the four groups of pixels is N and corresponds to the total number of pixels present in the image.

The Accuracy is the proportion of correct classified pixels relatively to the total number of pixels (Equation 4.1):

$$Accuracy = \frac{TP + TN}{N} \tag{4.1}$$

The Precision reflects the proportion of predicted positive pixels which are in fact real positives cases 4.2:

$$Precision = \frac{TP}{TP + FP} \tag{4.2}$$

Recall, also known as Sensitivity, denotes the proportion of real positive pixels which are correctly stated as positive, measuring the coverage of the realistic positive cases 4.3:

$$Recall = \frac{TP}{TP + FN} \tag{4.3}$$

The Dice Score Coefficient, also known as F-measure, F-score or even F1-score, appears in order to combine this last two measures which, despite relating the positive examples and predictions, do not reflect the false classifications, considered as errors, or even the well discarded pixels. It is the Harmonic mean of the two metrics, taking both false positives and false negatives into account (Equation 4.4):

$$DSC = 2\frac{Recall \cdot Precision}{Precision + Recall} \tag{4.4}$$

It quantifies the true positive area in ground truths relating it to incorrectly covered or missed. From all four performance measures, the DSC provides more balance in the pixel classification relationship, in the way that it is a weighted measure making it the most important value when each solution and optimization were being sought in this work [Yang and Liu, 1999, Powers, 2011].

4.2.1 Classification Methods

The classification based methods parameters were optimized in order to be adapted and empowered their results. The SVM based algorithm parameters, applied to both set of features involved the addition of lower cycle frequencies in order to expand the set of Gabor filters, the addition of location and intensity features and the evaluation of the impact of each new set of features on the results. The tested set of cycles was [0.001-2], the location was the x,y,z relative position in the image and intensity the normalized pixel values. Also, the number of folds in cross-validation was optimized, tested from 3 until 20 folds.

In the RF based algorithm the optimizations were made in the number of bagging trees used in the modeling phase, from 5 to 30. Also, the cross-validation folds were tested from the 3 to 20.

4.2.1.1   Sternum

Textural features

The results from the implementation of the proposed classification method in Bourgeat et al. [2007] to this MRI chest implementation and the best results obtained with the same features fundamentals are explicit in the following Table 4.1.

Table 4.1: Bourgeat et al. [2007] methodology implementation results for sternum identification.

	Original classification (SVM)	**SVM adaptation**	**RF adaptation**
Accuracy	0.758	0.856	0.805
Precision	0.054	0.074	0.050
Recall	0.194	0.107	0.098
DSC	0.081	0.083	0.065

The reproduction of the original classification algorithm did not pass the DSC of 0,08, its optimized adaptation had a DSC of 0.083 and the RF application a DSC of 0.065.

The SVM adaption was reached using the same frequencies for Gabor filtering and combining them with smaller frequencies [0.04; 0.033; 0.02; 0.01; 0.005; 0.0025]. The same k-fold value for cross-validation, 5, was used. In the RF optimization, the number of bagging trees used was 20 with a 10-fold cross-validation, with the original set of features.

Statistical, edge and location features

From the application of the proposed method in Balsiger et al. [2015] and the application of the same features varying parameters and the method of classification, the best results obtained were the followings presented in the Table 4.2

Table 4.2: Balsiger et al. [2015] methodology implementation results for sternum segmentation.

	Original classification (RF)	**RF adaptation**	**SVM adaptation**
Accuracy	0.741	0.739	0.783
Precision	0.035	0.035	0.048
Recall	0.078	0.083	0.247
DSC	0.048	0.048	0.087

The RF original algorithm reproduction, in this context, only achieved a DSC of 0.048. The method optimization had a DSC of 0.048 and the SVM adaptation using this set of features a DSC of 0,087.

The optimized adaptation of the RF model was achieved using 10 bagging trees and the SVM with a 15-fold cross-validation.

4.2.1.2   Clavicles

Textural features

The results from the directly application of the proposed method in Bourgeat et al. [2007] and the posterior optimizations using the same set of extracted features are explicit in the following Table 4.3.

Table 4.3: Bourgeat et al. [2007] methodology implementation results for clavicle identification.

	Original classification (SVM)	SVM adaptation	RF adaptation
Accuracy	0.609	0.586	0.755
Precision	0.163	0.158	0.181
Recall	0.421	0.440	0.206
DSC	0.233	0.235	0.190

The DSC for the original algorithm is 0.233, its optimization 0.235 and the RF performance was 0.192. The optimization using the same classification method, SVM, was achieved with the modification of the fold value in cross-validation, setting it to 7. The best result achieved using the RF classifier was accomplished with the same set of features and setting the number of bagging trees to 20.

Statistical, edge and location features

The implementation of the Balsiger et al. [2015] algorithm to identify the Clavicles and the optimized results using the same set of features modifying the parameters and the classification method is present in the following Table 4.4.

Table 4.4: Balsiger et al. [2015] methodology implementation results for Clavicles identification.

	Original classification (RF)	RF adaptation	SVM adaptation
Accuracy	0.746	0.699	0.620
Precision	0,194	0.177	0.150
Recall	0.252	0.307	0.732
DSC	0.216	0.222	0.246

The optimization maintaining the RF classification method was accomplished changing the number of bagging trees to 5. The same set of features but classified with SVM achieved the best result with a 5-fold cross-validation.

4.2.2 Gradient Based Segmentation

In the following sections, the final results from the gradient based algorithm implementation are presented. This approach does not require a training set to adjust a classification model. However, in order to be provide an equal comparison to the previous methods, the results were optimized in the training dataset and tested in the test dataset, being presented separately.

4.2.2.1 Sternum

Some examples from the minimum path cost estimation are presented on Sternum ROIs in the following images (Figures 4.1 to 4.3).
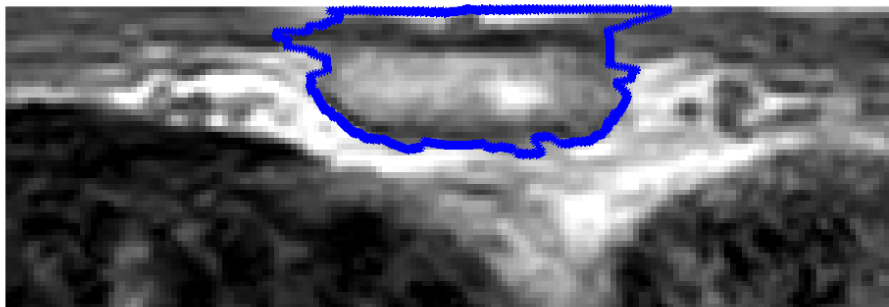

Figure 4.1: Minimum path result for sternum contour fisrt example.

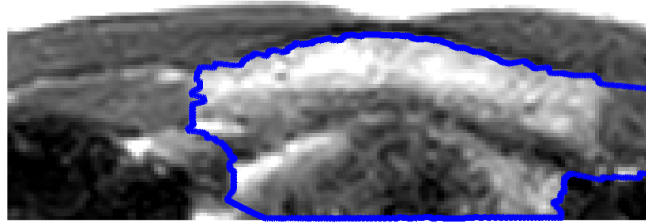Figure 4.2: Minimum path result for sternum contour second example.

Figure 4.3: Minimum path result for sternum contour third example.

The results from the gradient minimum cost pixels path based algorithm applied to the sternum identification are explicit in the following Table 4.5.

Table 4.5: Gradient based sternum segmentation results.

	Training Set	Test Set
Accuracy	0.887	0.877
Precision	0.459	0.515
Recall	0.487	0.654
DSC	0.450	0.575

The developed algorithm performance in the 10 training set acquisitions, the DSC was 0.450 increasing to 0.575 when applied to the 4 acquisitions test set.

4.2.2.2   Clavicles

Some examples from the minimum path algorithm in clavicles ROIs are presented in the following images (Figures 4.4 to 4.6).
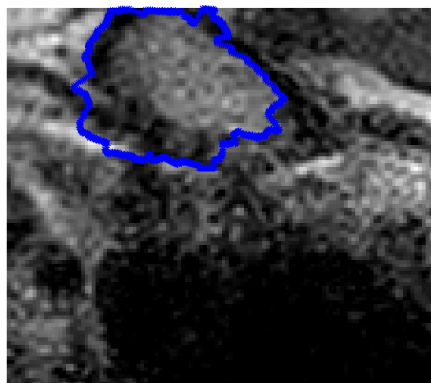

Figure 4.4: Minimum path result for clavicle contour first example.

Figure 4.5: Minimum path result for clavicle contour second example.
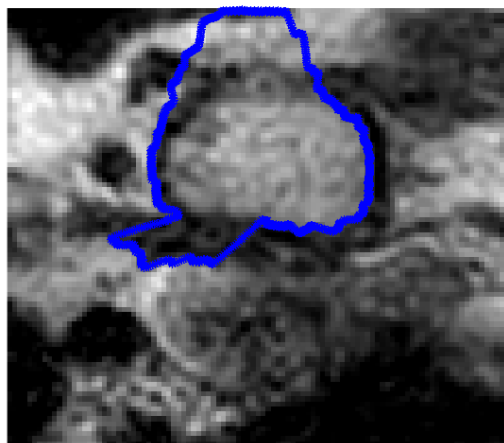
Figure 4.6: Minimum path result for clavicle contour thrid example.

The results from the gradient based minimum path algorithm are shown in the following Table 4.6. The minimum path approach performance DSC was of 0.185 for the training set. In the test set it increased to a DSC of 0.359.

Table 4.6: Minimum path result for clavicle contour example.

	Training Set	Test Set
Accuracy	0.766	0.838
Precision	0.122	0.3112
Recall	0.384	0.424
DSC	0.185	0.359

4.3 Discussion

The obtained results, explicit in the previous Section 4.2 must be compared and discussed in order to realize the differences between the methods and the algorithms responses to the MRI acquisitions. The SVM classification reproduced method, in its original study achieved a DSC of 0.87. The RF based method a DSC of 0.92.

In the Gradient based segmentation, the method was not a truly reproduction of any described algorithms, only inspired in Oliveira et al. [2012], Teixeira and Oliveira [2017] and adapted to the type of images and objects to be segmented. The only comparison possible is with the classification based methods.

4.3.1 Classification Methods

The Classification methods, despite having tried several set of features and two distinct learning models, did not achieve results that can be considered solutions for the object identification problems.

In Figures 4.7 and 4.8 a compilation of example results for sternum and clavicles are shown. The SMV based approach achieved a low DSC of about 0.08 and the RF did not pass 0.07, which is considerably below the described results, 0.87 and 0.92 respectively, in the original applications.

The low performance of both classifiers can be related to the object's characteristics and their surroundings, which are very alike in some slices and can compromised the learning processes of the classifiers. The heterogeneity of the objects to be identified, specially the sternum, may also compromises the learning training phase.
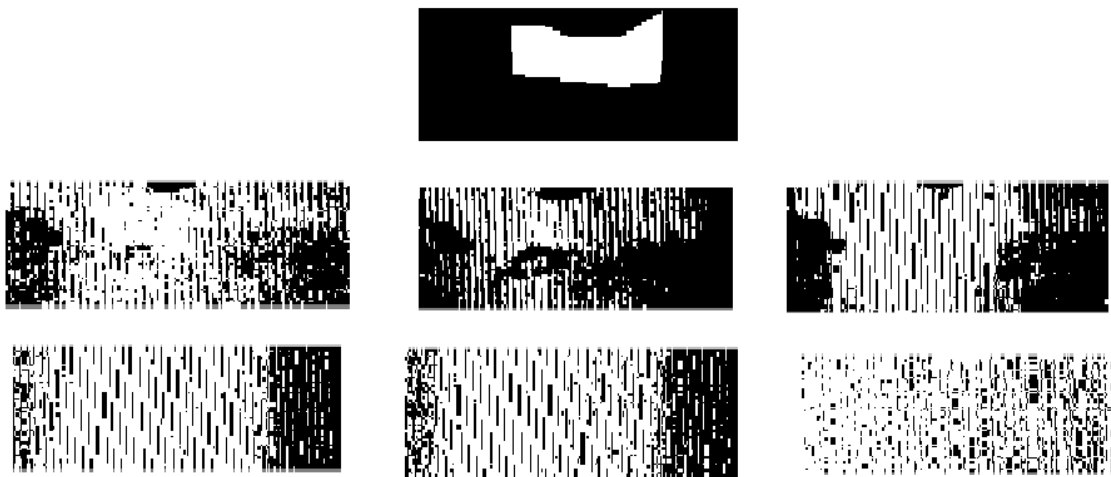

Figure 4.7: SVM and RF classification methods in Bourgeat et al. [2007] and Balsiger et al. [2015] features results in sternum compared to the ground truth.
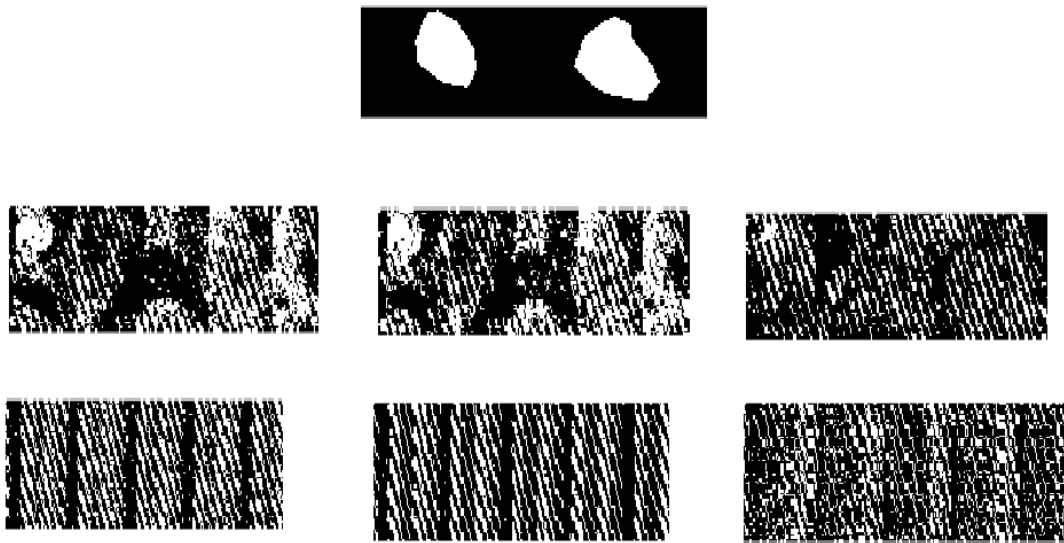
Figure 4.8: SVM and RF classification methods in Bourgeat et al. [2007] and Balsiger et al. [2015] features results in clavicles compared to the ground truth.

4.3.2 Gradient Based Segmentation

The solution here presented was the algorithm with best performance of the experiments. Although the DSC does not pass 0.6, in sternum segmentation, and 0.36 in clavicle, it representsa considerable improvement concerning the results of the previous experiments. On the other hand, despite the Accuracy values being high (about 0.9), relating them with the other metric values reflects an over-segmentation, meaning that many False Positives are being highly detected (Figures 4.9 to 4.10).

The large number of steps taken to reach the segmentation results can boost multiple sources of procedure errors. The step that precedes the elliptical parameters estimation is made based on rough masks, whose object identification often fails. This leads to the necessity of inter and extrapolated the parameters, for those missing slices. If many slices fail the initial threshold, or even if it is not the adequate identification, the error will be propagated to the other elliptical parameter's estimation and consequently to the image's transformation.

This segmentation method takes many steps to be accomplished. Each step taken is a potential error propagation source, from the ROI estimation to the minimum path determination or even the reversion of the elliptical deformation, causing a change in the object contours identification. Every step that leads to the desired aim can also compromise the object segmentation.
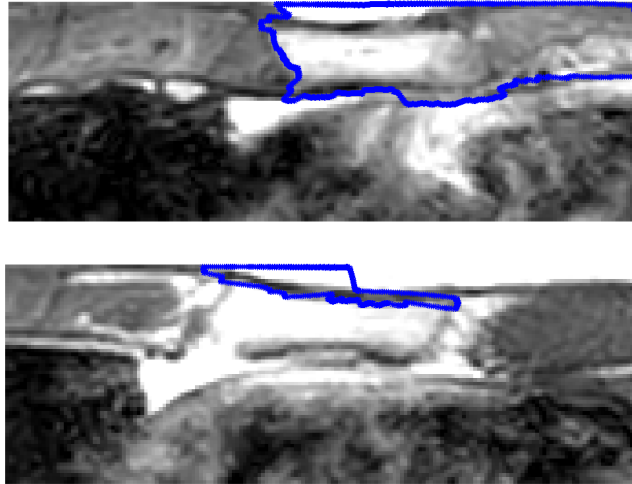
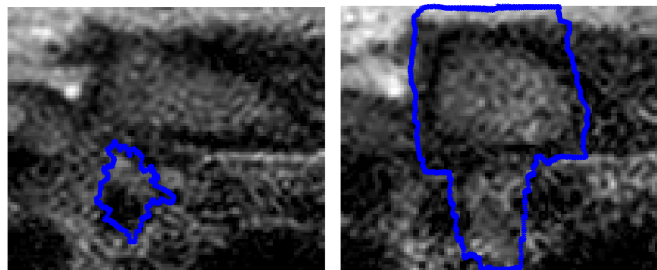Figure 4.9: Minimum paths missing sternum contours.

Figure 4.10: Minimum paths missing clavicle contours.

Chapter 5

Conclusions and Future Work

5.1 Conclusions

In this dissertation, a method using gradient based minimum path calculation for sternum and clavicles detection in MRI is proposed. This method achieves the desired bone contours, in T1-weighted acquisitions without needing the user intervention. Its performance was evaluated by calculating Accuracy, Precision, Recall and DSC. The algorithm developed represents a relevant improvement for the sternum and clavicles segmentation in MRI. Despite having over and under segmentation, especially in clavicle detection, their main purpose, to serve as keypoint for the 3D modeling, is possible. Other methods, such as based on classification were experimented, though these did not amount to significant results.

The bone shapes and the dual presence of clavicles constituted major differences about the structures. The clavicles, unlike the sternum that shows up uniquely and in most of the MRI slices, only appear in the upper images.

The fact that this method automatically identifies the ROI, it sharpens the object identification area, limiting where the it should be identified. Meaning that, even the false detected pixels are reasonably close the intended objects.

The essential objective of the work is the bones detected can serve as keypoints for the 3D modeling.

The outcomes should be interpreted within the context of study limitations. Firstly, the dataset used was quite small to state unequivocally that the presented solution is a robust MRI segmentation method.

Then, the heterogeneity of the objects in the acquisitions used, across slices and between different patients, perhaps prevented the classification models to properly adjust to the manifold examples given during the training phase.

Another limitation for the method robustness is the diversity of clavicle appearances, differing sometimes in shape and position between each side in the same slice. The presence of the sternum also varies in the number of slices per acquisition from patient to patient.

Finally, a big limitation for the progress of this project was the unavailability of the reproduced classification methods, specially the texture based algorithm, whose descriptions on the publications were quite ambiguous in some steps. Linked to the time restriction of this kind of studies, this was one of the biggest obstacles during this course.

Despite the limitations mentioned above, this work achievements were a novelty in the biomedical imaging field, contributing for the MRI bone segmentation studies. It could inspire other image scientists to launch themselves in this area. In addition, it can be a good starting point for others who want to study this segmentation techniques or MRI bone chest detection.

5.2   Future Work

Future studies should explore the subjects previously referred as limitations. Evaluating the results in a larger MRI dataset will enrich the study of this solution as viable for these purposes.

Furthermore, the sternum and clavicles MRI identification in the proposed method can be empowered with the reduction of steps to achieve the elliptical transformation. Even with the use of a more refined method to primarily identify the objects shape, before the elliptical parameters' estimation, would probably enhance the results.

Additionally, other classification methods could be tried using the same features tested in the present work.

Based on the described methods for leg segmentation, the design of statistical shape models should be an approach to consider for posterior bone segmentation in this MRI context or even completely different approaches from the ones mentioned.

References

Sufyan Y Ababneh, Jeff W Prescott, and Metin N Gurcan. Automatic graph-cut based segmentation of bones from knee magnetic resonance images for osteoarthritis research. *Medical image analysis*, 15(4):438–448, 2011.

Fabian Balsiger, Tiziano Ronchetti, and Martin Pletscher. Distal femur segmentation on MR images using random forests. *Medical Image Analysis Laboratory 2015*, 2015.

P. Bourgeat, S. Ourselin, P. Stanwell, and S. Ramadan. Texture-Based Segmentation of the Knee Bones in MRI Using Phase Information. In *3rd IEEE International Symposium on Biomedical Imaging: Macro to Nano, 2006.*, pages 742–745. IEEE, 2006. ISBN 0-7803-9576-X. doi: 10.1109/ISBI.2006.1625023. URL http://ieeexplore.ieee.org/document/1625023/.

Pierrick Bourgeat, Jurgen Fripp, Peter Stanwell, Saadallah Ramadan, and Sébastien Ourselin. MR image segmentation of the knee bone using phase information. *Medical Image Analysis*, 11(4): 325–335, aug 2007. ISSN 1361-8415. doi: 10.1016/J.MEDIA.2007.03.003. URL https://www.sciencedirect.com/science/article/pii/S1361841507000291.

Leo Breiman. Random forests. *Machine Learning*, 45(1):5–32, 2001. ISSN 08856125. doi: 10.1023/A:1010933404324.

John Canny. A Computational Approach to Edge Detection. *IEEE Transactions on Pattern Analysis and Machine Intelligence*, PAMI-8(6):679–698, nov 1986. ISSN 01628828. doi: 10.1109/TPAMI.1986.4767851. URL http://ieeexplore.ieee.org/lpdocs/epic03/wrapper.htm?arnumber=4767851.

Vicent Caselles, Ron Kimmel, and Guillermo Sapiro. Geodesic Active Contours. *International Journal of Computer Vision*, 22(1):61–79, 1997. ISSN 09205691. doi: 10.1023/A:1007979827043. URL http://link.springer.com/10.1023/A:1007979827043.

Constance D. Lehman Christoph I. Lee and Lawrence W. Bassett. *Breast Imaging*. Number 781. Oxford University Press, 2018. ISBN 9780190270261. doi: 10.1093/med/9780190270261.001.0001.

Rupin Dalvi, Rafeef Abugharbieh, DerekC Wilson, and David R Wilson. Multi-contrast MR for enhanced bone imaging and segmentation. In *Engineering in Medicine and Biology Society, 2007. EMBS 2007. 29th Annual International Conference of the IEEE*, pages 5620–5623. IEEE, 2007.

Erik B Dam, Martin Lillholm, Joselene Marques, and Mads Nielsen. Automatic segmentation of high-and low-field knee MRIs using knee image quantification with data from the osteoarthritis initiative. *Journal of Medical imaging*, 2(2):024001–024001, 2015.

Jurgen Fripp, Stuart Crozier, Simon K Warfield, and Sebastien Ourselin. Automatic segmentation of the bone and extraction of the bone–cartilage interface from magnetic resonance images of the knee. *Physics in Medicine and Biology*, 52(6):1617, 2007.

Akash Gandhamal, Sanjay Talbar, Suhas Gajre, Ruslan Razak, Ahmad Fadzil M Hani, and Dileep Kumar. Fully automated subchondral bone segmentation from knee MR images: Data from the osteoarthritis initiative. *Computers in Biology and Medicine*, 88:110–125, 2017.

Yanrong Guo, Jianguo Jiang, Shijie Hao, and Shu Zhan. Distribution-based active contour model for medical image segmentation. In *Image and Graphics (ICIG), 2011 Sixth International Conference on*, pages 61–65. IEEE, 2011.

Maria Cristina Ferrarini Nunes Soares Hage and Masao Iwasaki. Imagem por ressonância magnética: princípios básicos. *Ciência Rural*, 39(4):1275–1283, 2009.

Tal Hendel. Ellipse Fit - File Exchange, 2008. URL https://www.mathworks.com/matlabcentral/fileexchange/22423-ellipse-fit?focused=5109545{&}tab=function.

Matthias Hofmann, Ilja Bezrukov, Frederic Mantlik, Philip Aschoff, Florian Steinke, Thomas Beyer, Bernd J Pichler, and Bernhard Schölkopf. MRI-based attenuation correction for whole-body pet/mri: quantitative evaluation of segmentation-and atlas-based methods. *Journal of Nuclear Medicine*, 52(9):1392–1399, 2011.

Anil Jain, Karthik Nandakumar, and Arun Ross. Score normalization in multimodal biometric systems. *Pattern Recognition*, 38(12):2270–2285, dec 2005. ISSN 0031-3203. doi: 10.1016/J.PATCOG.2005.01.012. URL https://www.sciencedirect.com/science/article/pii/S0031320305000592.

Jian-Guo Jiang, Yanrong Guo, Shu Zhan, and Hong Li. Segmentation of knee joints based on improved multiphase chan-vese model. In *Bioinformatics and Biomedical Engineering, 2008. ICBBE 2008. The 2nd International Conference on*, pages 2418–2422. IEEE, 2008.

F. Jin, P. Fieguth, L. Winger, and E. Jernigan. Adaptive Wiener filtering of noisy images and image sequences. *Proceedings 2003 International Conference on Image Processing (Cat. No.03CH37429)*, 2(1):III–349–52, 2003. ISSN 1522-4880. doi: 10.1109/ICIP.2003.1247253. URL http://ieeexplore.ieee.org/document/1247253/.

Georgia College & State University Ken Saladin. *Anatomy & Phisiology: The Unit of Form and Function*. The McGraw-Hill Companies, 3rd edition, 2003. ISBN 0072919264. doi: 10.15713/ins.mmj.3.

June-Goo Lee, Serter Gumus, Chan Hong Moon, C. Kent Kwoh, and Kyongtae Ty Bae. Fully automated segmentation of cartilage from the mr images of knee using a multi-atlas and local structural analysis method. *Medical Physics*, 41(9), aug 2014. ISSN 00942405. doi: 10.1118/1.4893533. URL http://doi.wiley.com/10.1118/1.4893533.

Wenzhu Lu, Jianhua Yao, Chao Lu, Sheila Prindiville, and Catherine Chow. DCE-MRI segmentation and motion correction based on active contour model and forward mapping. In *Software Engineering, Artificial Intelligence, Networking, and Parallel/Distributed Computing, 2006. SNPD 2006. Seventh ACIS International Conference on*, pages 208–212. IEEE, 2006.

Bill McNeese. Are the Skewness and Kurtosis Useful Statistics? | BPI Consulting, 2016. URL https://www.spcforexcel.com/knowledge/basic-statistics/are-skewness-and-kurtosis-useful-statistics.

Andrew Mehnert and Paul Jackway. An improved seeded region growing algorithm. *Pattern Recognition Letters*, 18(10):1065–1071, oct 1997. ISSN 0167-8655. doi: 10.1016/S0167-8655(97)00131-1. URL https://www.sciencedirect.com/science/article/pii/S0167865597001311.

Tuhina Neogi, Michael A Bowes, Jingbo Niu, Kevin M Souza, Graham R Vincent, Joyce Goggins, Yuqing Zhang, and David T Felson. Magnetic resonance imaging-based three-dimensional bone shape of the knee predicts onset of knee osteoarthritis: data from the osteoarthritis initiative. *Arthritis & Rheumatology*, 65(8):2048–2058, 2013.

Hélder P. Oliveira, Jaime S. Cardoso, André Magalhães, and Maria J. Cardoso. Simultaneous detection of prominent points on breast cancer conservative treatment images. *Proceedings - International Conference on Image Processing, ICIP*, pages 2841–2844, 2012. ISSN 15224880. doi: 10.1109/ICIP.2012.6467491.

Hélder P. Oliveira, Jaime S. Cardoso, André T. Magalhães, and Maria J. Cardoso. A 3D low-cost solution for the aesthetic evaluation of breast cancer conservative treatment. *Computer Methods in Biomechanics and Biomedical Engineering: Imaging and Visualization*, 2(2):90–106, 2014. ISSN 21681171. doi: 10.1080/21681163.2013.858403.

Nobuyuki Otsu. A Threshold Selection Method from Gray-Level Histograms. *IEEE Transactions on systems, Man and Cybernetics.*, 20(1):62–66, 1979. ISSN 0018-9472. doi: 10.1109/TSMC.1979.4310076.

Firat Ozdemir, Neerav Karani, Philipp Fürnstahl, and Orcun Goksel. Interactive segmentation in MRI for orthopedic surgery planning: bone tissue. *International Journal of Computer Assisted Radiology and Surgery*, pages 1–9, 2017.

Harold E. Paul B, Adam M. *Applied Radiological Anatomy for Medical Students*. Cambridge University Press, 2007. ISBN 9780874216561. doi: 10.1007/s13398-014-0173-7.2.

David M.W. Powers. EVALUATION: FROM PRECISION, RECALL AND F-MEASURE TO ROC, INFORMEDNESS, MARKEDNESS & CORRELATION. *Journal of Machine Learning Technologies*, 2(1):37–63, 2011. ISSN 2229-3981. URL http://dspace.flinders.edu.au/dspace/http://www.bioinfo.in/contents.php?id=51.

Donna M. Reeve. Breast mri and quality control, 2018. URL https://pdfs.semanticscholar.org/presentation/8d41/a277e4291929ae0591da300d533187650643.pdf.

Trent Stephens Rod Seeley and Philip Tate. *Anatomy & Phisiology*. McGraw-Hill Companies, 6th edition, 2003. ISBN 0073109428.

Jérôme Schmid, Jinman Kim, and Nadia Magnenat-Thalmann. Robust statistical shape models for mri bone segmentation in presence of small field of view. *Medical image analysis*, 15(1):155–168, 2011.

J.A.K. Suykens and J. Vandewalle. Least Squares Support Vector Machine Classifiers. *Neural Processing Letters*, 9(3):293–300, 1999. ISSN 13704621. doi: 10.1023/A:1018628609742. URL http://link.springer.com/10.1023/A:1018628609742.

João F. Teixeira and Hélder P. Oliveira. Spacial Aliasing Artefact Detection on T1-Weighted MRI Images. *Springer International Publishing AG 2017*, 10255:462–470, 2017. doi: 10.1007/978-3-319-58838-4. URL http://link.springer.com/10.1007/978-3-319-58838-4.

Eralci Moreira Therézio, Gustavo G. Dalkiranis, André A. Vieira, Hugo Gallardo, Ivan H. Bechtold, Patricia Targon Campana, and Alexandre Marletta. Achromatic Ellipsometry: Theory and Applications. In *Ellipsometry - Principles and Techniques for Materials Characterization*. InTech, nov 2017. doi: 10.5772/intechopen.70089. URL http://www.intechopen.com/books/ellipsometry-principles-and-techniques-for-materials-characterization/achromatic-ellipsometry-theory-and-applications.

Eric W. Weisstein. Ellipse. *MathWorld-A Wolfram Web Resource*, 2018. URL http://mathworld.wolfram.com/Ellipse.html.

Yiming Yang and Xin Liu. A re-examination of text categorization methods. *Proceedings of the 22nd annual international ACM SIGIR conference on Research and development in information retrieval - SIGIR '99*, pages 42–49, 1999. ISSN 1581130961. doi: 10.1145/312624.312647. URL http://portal.acm.org/citation.cfm?doid=312624.312647.